始生代グリーンストン帯の形成過程

課題番号：07640638

平成７年度～平成８年度科学研究費補助金（基盤研究(C)(2)）
研究成果報告書

平成９年３月

研究代表者：星野　光雄
（名古屋大学情報文化学部助教授）

はしがき

本研究は、平成７年度と８年度の２年間にわたり、文部省科学研究費の助成を受けて実施されたものである。本研究の目的は以下のようにまとめられる。

グリーンストン帯は始生代クラトンを特徴づける地質体であり、プロト大陸であると考えられる。グリーンストン帯には共通して、下位火山岩層－上位砕屑性堆積岩相－後造山期花崗岩体の岩相組合わせが認められる。このようなきわめて特異なグリーンストン帯を形成した地球初期の地質過程とはどのような性格のものであったのかを解明する。

私どもは本研究を、上記の目的を達成するための第一段階として捉え、ケニアのグリーンストン帯に焦点を絞って、そこにみられる後造山期花崗岩貫入にともなう熱変成作用の岩石学的解析からグリーンストン帯形成当時の熱構造を明らかにしようと試みた。さらに、本研究の特徴として、火成岩類の産状や地質構造など、私どもが今までに積み重ねてきた地質学的現地調査に立脚して行われることが挙げられる。

本研究の室内実験に関する主な研究方法は、岩石の蛍光Ｘ線分析 (XRF)、鉱物のＸ線マイクロアナライザー分析 (EPMA)、岩石の顕微鏡観察である。これらの室内実験に供する岩石試料は1991年現地調査（日本学術振興会助成金）および1994年現地調査（社団法人東京倶楽部助成金）で採集したものを使用した。このたびの科学研究費については、XRF分析のためのJEOL JK-40W1X型冷却水循環装置を設置、室内実験用消耗品類の購入、資料収集旅費が主な使途であり、ほぼ計画通りの実験が遂行できた。

なお、本研究成果はその一部を学会で口頭発表し、また平凡社地学事典の全面改訂に際して大きく貢献した。論文としては現在投稿中のものがあり、さらにもう一つの論文を準備中である。

謝辞：本研究は文部省科学研究費補助金（基盤研究(C)(2)、課題番号07640638）により遂行された。文部省および名古屋大学の関係各位に感謝申し上げる。また、分析用岩石薄片を多数作成してくださった名古屋大学文部技官の長岡　勉氏にも感謝申し上げたい。

研究組織

研究代表者：　星　野　光　雄　（名古屋大学情報文化学部　助教授）
研究分担者：　伊　藤　正　裕　（名古屋大学情報文化学部　教授）
研究分担者：　杉　谷　健　一　郎　（名古屋大学情報文化学部　助手）

研究経費

平成７年度	１,７００千円
平成８年度	６００千円
計	２,３００千円

研究発表

(1)　学会誌等

Opiyo-Akech, N. and Hoshino, M.: Petrology, geochemistry and petrogenesis of some Archaean granites from the Archaean Greenstone Belt to the north of Lake Victoria, Western Kenya.　Jour. Afr. Earth Sci. (発表予定)

(2)　口頭発表

星野光雄・澤田順弘・諏訪兼位:「ケニアの地質と表層環境」.　第32回日本アフリカ学会学術大会研究発表要旨, 54, 1995年5月.

星野光雄・澤田順弘・諏訪兼位・佐藤 俊:「北ケニア,コル地域産砂漠砂の鉱物学」. 第33回日本アフリカ学会学術大会研究発表要旨, 58, 1996年5月.

(3)　出版物

地学団体研究会:「新版地学事典」. 平凡社, 1996年10月.（先カンブリア時代・アフリカ　星野光雄,項目執筆）

研究成果

1．地質概説

アフリカ大陸には先カンブリア時代の岩相が広汎に露出する。これらのうちでも25億年より古い始生代の岩層を主体とし、それ以降の造山運動をほとんど被っていない安定地塊をクラトンと呼ぶ。そのひとつタンザニア・クラトンは東アフリカに位置し、東北端部がケニア西部のビクトリア湖岸一帯にみられる（Fig. 1）。タンザニア・クラトンの東側はモザンビーク帯と接し、原生代中期～後期の造山運動により形成された変成岩・花崗岩層が南北方向のトレンドで露出している。モザンビーク帯の中央部には第三紀以降に形成され現在も活動中のアフリカ大地溝帯が発達する。

タンザニア・クラトン全体をながめると、中部～南部には片麻岩－花崗岩の組合せで特徴づけられる岩層が卓越し、片麻岩はグラニュライト相に達する高度の広域変成作用を被っている。一方、本研究地域を含む北部一帯は火山岩－砕屑性堆積岩－花崗岩の組合わせで特徴づけられ、広域変成作用の変成度はきわめて低く、むしろ花崗岩の貫入に伴う熱変成作用が顕著である。なおグリーンストン帯の名前の由来は、玄武岩、安山岩を大量に含む火山岩層が全体的に緑色を呈することによる。

Hoshino et al. (1983) による地質図 (Fig. 1) にもとづいてケニア西部のグリーンストン帯の地質を以下に概説する。始生代の岩層は古い順にニアンザ系 (Nyanzian System)、カビロンド系 (Kavirondian System)、花崗岩類 (Granitic rocks) より構成される。最下部のニアンザ系は玄武岩、安山岩、流紋岩の火山岩類よりなり、全層厚は数千mと見積もられる。玄武岩、安山岩の多くは low-K ソレアイト系列に属し、一部はカルク-アルカリ岩系列に属する (Suwa, 1981)。カビロンド系はニアンザ系を不整合に覆い、礫岩、砂岩、泥岩などの砕屑性堆積岩よりなる。全層厚は数千m以上と見積もられる。ニアンザ系、カビロンド系ともに緩やかな褶曲構造を示し、褶曲軸のトレンドは東北東－西南西である。本地域の南部において上記両系は第三紀のフォノライトに覆われる。花崗岩類はニアンザ系、カビロンド系に貫入し、さまざまな岩相を呈する。主要な岩体としては、バソリス状のマラゴリ花崗岩 (Maragoli granite)、アセンボ花崗岩 (Asembo granite) およびムミアス花崗岩 (Mumias granite) が認められ、その他、マラゴリ花崗岩とアセンボ花崗岩の中間に位置する細粒花崗岩

(Micro granite) や小岩体として閃緑岩 (Diorite) が認められる (Opiyo-Akech and Hoshino, submitted)。花崗岩体の伸長方向は褶曲軸の方向とおおむね一致し、背斜軸部に集中している。この事実は、花崗岩の貫入と褶曲運動とが密接な関係にあることを示している。

Rb-Sr 放射年代測定の結果 (Yanagi and Suwa, 1981)は、ニアンザ系が28億年前、カビロンド系が26億年前、花崗岩類が25億年前に形成された岩層であることを示している。

2．熱変成作用

ニアンザ系、カビロンド系岩石類は広域変成作用を被っているが、その変成度は低く、原岩の組織をよく保存している。一方、花崗岩体の貫入による熱変成作用はきわめて明瞭である。ニアンザ系玄武岩、安山岩の鉱物組合せの変化を顕微鏡観察によって詳細に調べた結果を鉱物消長関係で示すと Table 1. のようになる。この結果にもとづいて変成分帯を行うことが可能である。即ち、変成度の低い順に、緑泥石－方解石－緑簾石－斜長石－石英の鉱物組合せで特徴づけられる Zone A、緑泥石－緑簾石－アクチノ閃石－斜長石－石英の鉱物組合せで特徴づけられる Zone B、ホルンブレンド－カミングトン閃石－単斜輝石－斜長石－石英の鉱物組合せで特徴づけられる Zone C の 3 帯が識別される。

それぞれの Zone の幅を地図上に示したものが Fig. 3 である。Zone C は花崗岩体との接触部からおおむね 3Km 以内に限られる。とくにバソリス状花崗岩体の周囲の Zone C は顕著であるが、小岩体の周囲では Zone C を欠くことがある。一方、Zone A は見掛け上褶曲構造の向斜軸とほぼ一致している。

熱変成作用を被った岩石中の鉱物の化学組成を決定するために、EPMA 分析を行った。分析は名古屋大学情報文化学部に設置されている Hitachi X-560 型 EPMA 分析装置を使用した。これまでに分析した鉱物の種類は、角閃石、白雲母、黒雲母、緑簾石および緑泥石である。これらの分析結果を Tables 2-6 に示しておく。

顕微鏡による鉱物記載および EPMA 分析結果にもとづいて、熱変成作用を相平衡論的に解析した結果をFig. 4 に示す。Zone A では緑簾石中のゾイサイト成分－緑泥石－方解石が共存し、下部緑色片岩相の変成度を示す。Zone B では緑簾石－緑泥石－

アクチノ閃石が共存し、上部緑色片岩相の変成度を示す。Zone C の高温部ではホルンブレンドーカミングトン閃石－単斜輝石－斜長石が共存し、上部角閃岩相の変成度を示す。

変成温度を示す情報は、残念ながらこれらの分析結果からは得られていない。ホルンブレンド単独の化学組成から推定される変成温度は、例えば 91100907 に含まれる褐色ホルンブレンドでおおよそ 750° と見積もられる。しかしこの推定は余り正確なものではなく、より精度の高い変成温度の推定のためにはさらに多くの鉱物の分析が必要である。

さらにこれらの分析結果から言えることは、同一岩石中の角閃石の組成が一定しない。即ち、熱変成作用は接触部付近においてさえ熱的平衡に達していなかったことを示唆するものである。

3．花崗岩類

花崗岩類についてのモード分析結果を Table 7 に示す。これによりマラゴリ花崗岩、アセンボ花崗岩および細粒花崗岩は明確に区分される。しかしムミアス花崗岩はアセンボ花崗岩に比較的近い。また、マラゴリ花崗岩と一部の細粒花崗岩は単斜輝石を含むことが特徴である。花崗岩類の詳細な岩石記載を Table 8 に示す。

花崗岩類の全岩化学組成を決定するために、XRF 分析を行った。分析には名古屋大学情報文化学部に設置されている JEOL JSX-601 型 XRF 分析装置を使用し、今回の科学研究費で購入した JEOL JK-40W1X 型冷却水循環装置を付属させた。分析結果を主要化学成分について Table 9 に示す。また、各成分の相関関係を Figs. 5-10 に示す。これらの相関図のあるものは、それぞれの岩型、とくにマラゴリ花崗岩とアセンボ花崗岩が比較的小範囲にまとまることを示すが、いくつかの相関図では各岩型内部でも組成上のまとまりを欠くことがある。とくにバソリス状の岩体のものと単独の小岩体のものとの間で顕著である。

4．まとめと今後の課題

本地域の熱変成作用の変成度は、接触部付近で上部角閃岩相を示すが、必ずしも熱的平衡には達していないと考えられる。また花崗岩体周囲の熱変成帯は小岩体ほど不規則である。さらに同一の岩体の中でも化学組成は比較的変化に富んでいる。

以上のことは、見掛け上同じ岩型のようにみえるものでも、それぞれ別の履歴をもつプルトンである可能性を示唆する。とくにバソリス状岩体と単独小岩体との間でそのことが言えるのではないだろうか。

今後の課題として、熱変成作用の詳細な温度の推定と温度分布の不規則性を明らかにすることと、花崗岩のバソリス状岩体と単独小岩体との間の履歴の違いを明らかにすることの二つが挙げられる。

参考文献

Hoshino, M., Yanagi, T., Suwa, K. and Winani, P. (1983): Geological structure of the Archaean greenstone belt, northwest of Kisumu, Kenya. 8th Prelim. Rept. Afr. Studies, Nagoya Univ., 145-156.

Opiyo-Akech, N. and Hoshino, M.: Petrology, geochemistry and petrogenesis of some Archaean granites from the Archaean Greenstone Belt to the north of Lake Victoria, Western Kenya. Jour. Afr. Earth Sci. (Submitted)

Suwa, K. (1981): Petrochemical and petrographical notes on some Nyanzian volcanic rocks, west Kenya. 6th Prelim. Rept. Afr. Studies, Nagoya Univ., 15-32.

Yanagi, T. and Suwa, K. (1981): Rb-Sr radiometric dating on Precambrian rocks in the western part of Kenya. 6th Prelim. Rept. Afr. Studies, Nagoya Univ., 163-172.

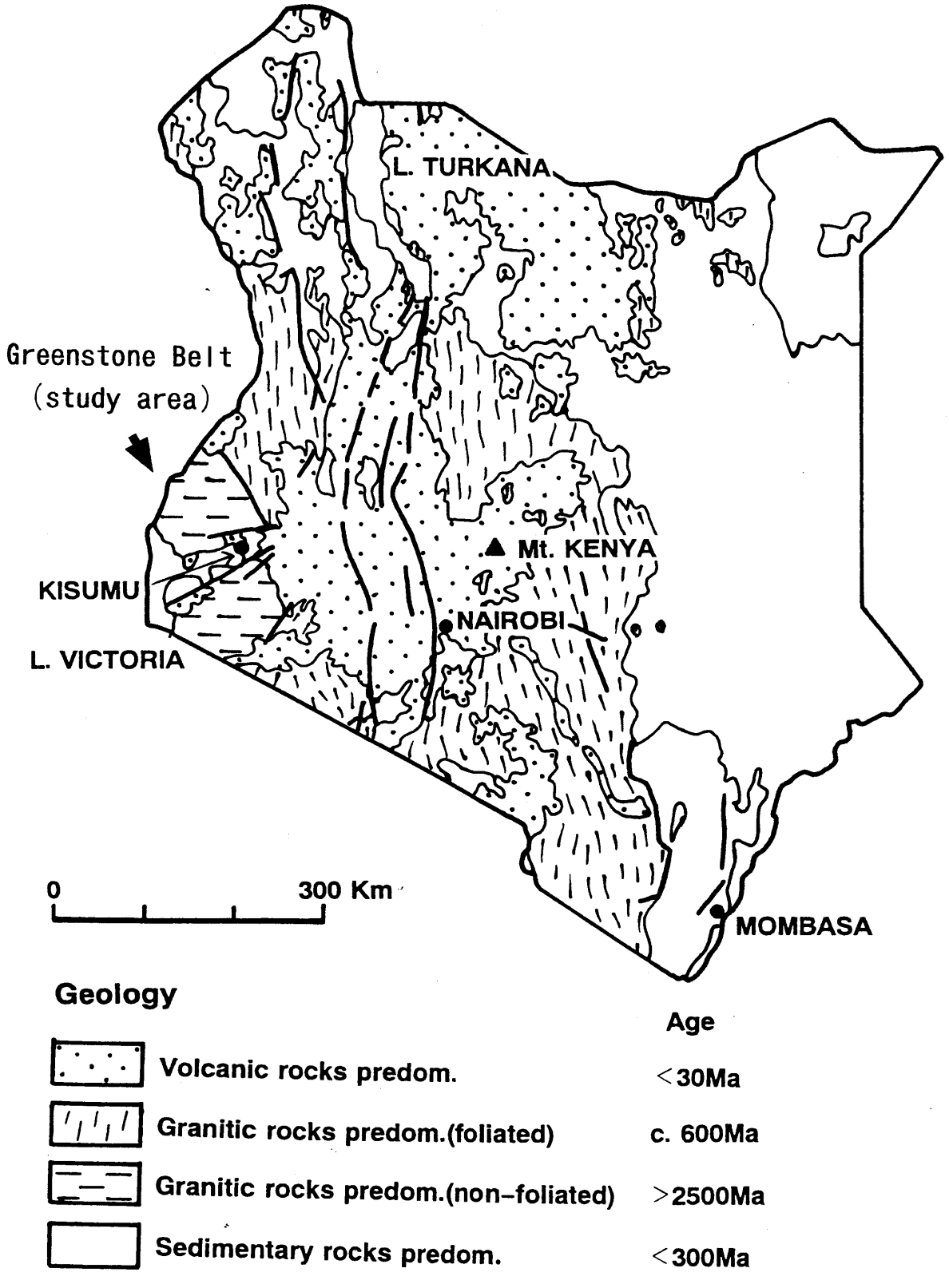

Fig. 1. Geological map of Kenya.

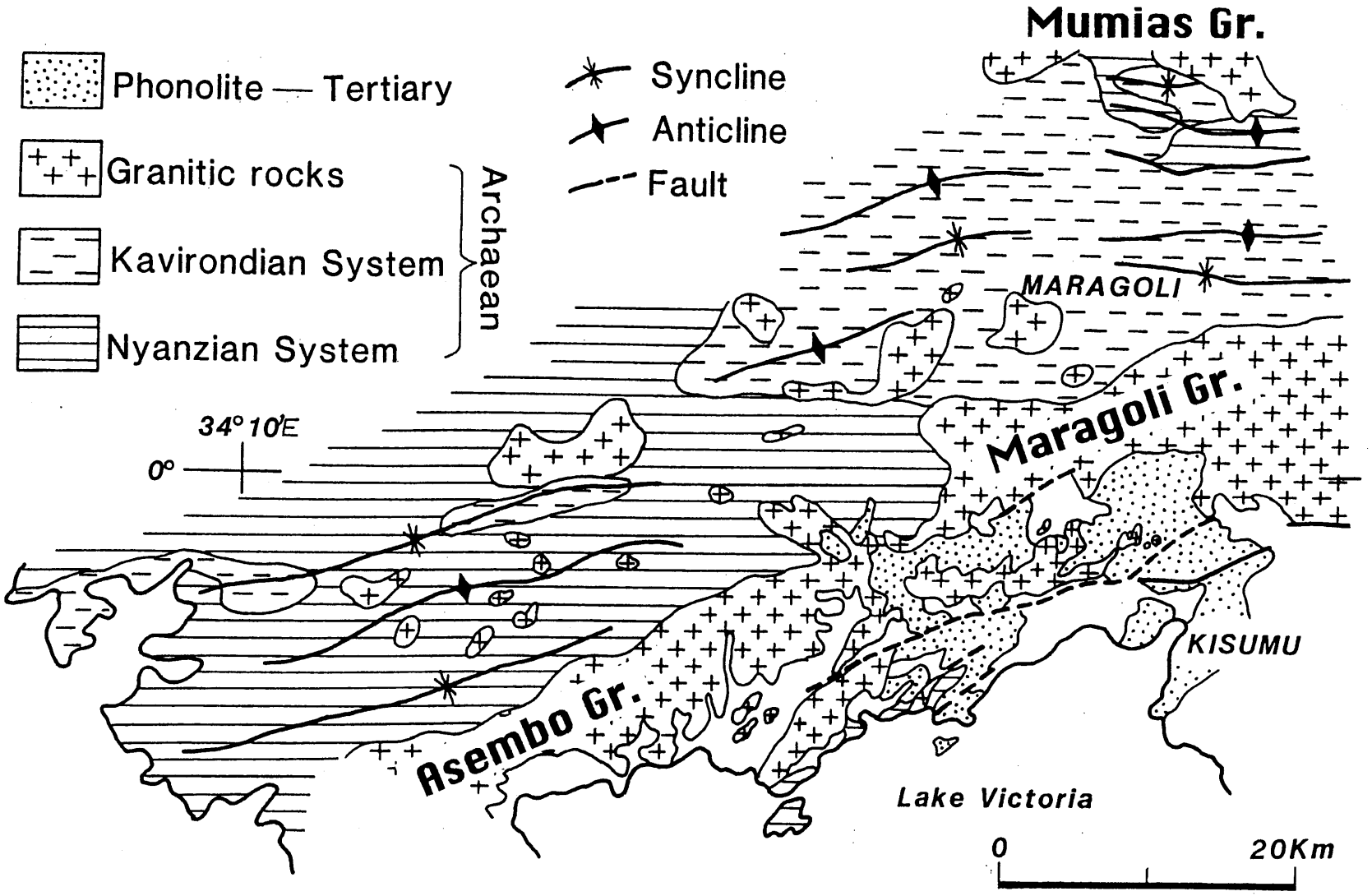

Fig. 2. Geological map of the Archaean Greenstone Belt, western Kenya.

Table 1. Mineral assemblages of the contact-metamorphosed mafic rocks.

Zone	A	B	C
Chlorite	———	———	
Calcite	———	———	
Epidote	———	———	———
Biotite		———	———
Actinolite	———	———	———
Hornblende			———
Cummingtonite			———
Clinopyroxene			———
Plagioclase	———	———	———
Quartz	———	———	———

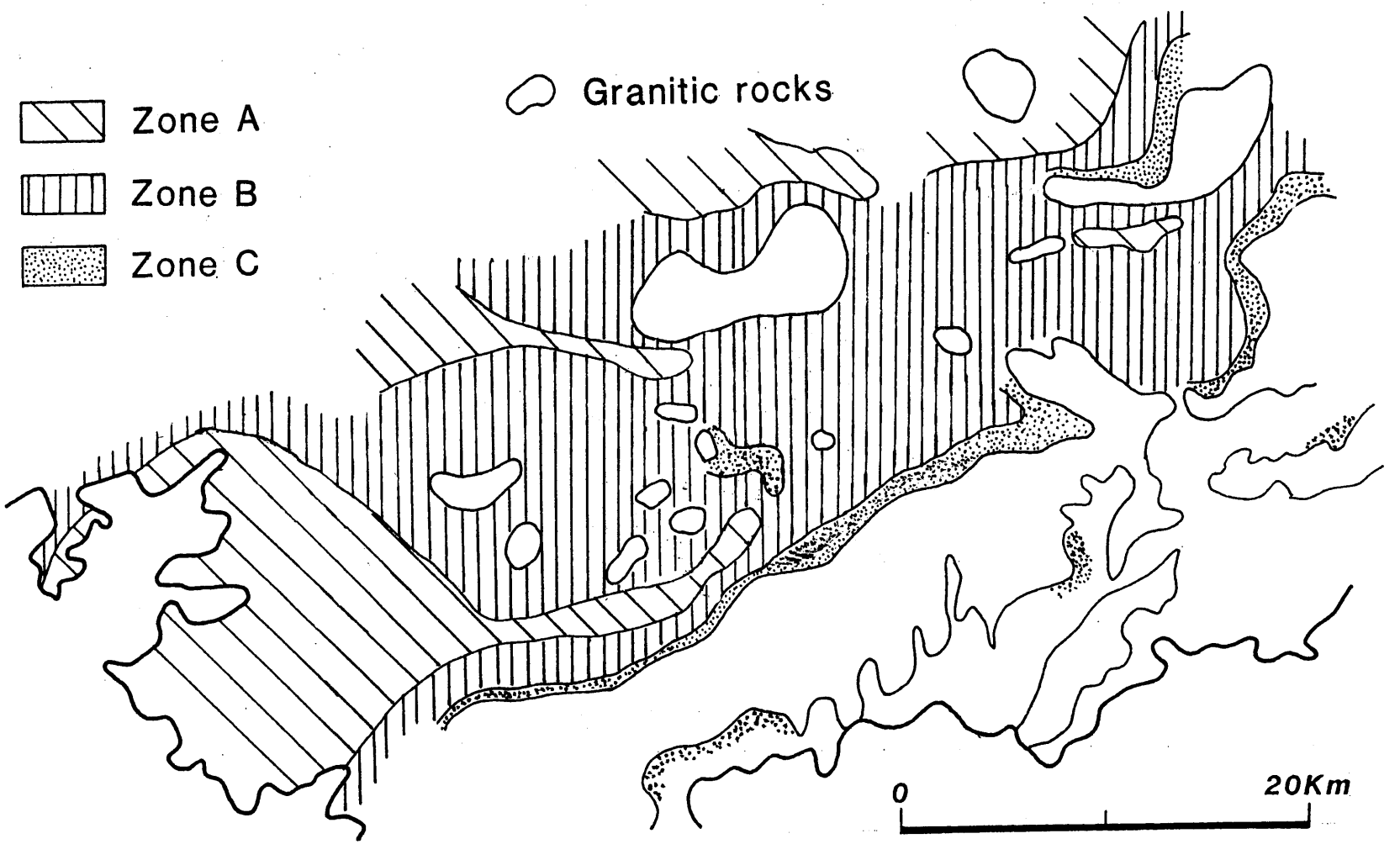

Fig. 3. Metamorphic zonation of the contact-metamorphosed rocks.

Table 2. Representative EPMA analyses of amphibole.

Sample no.	91101506	91100902	91100902	91100902
Colour+	Bl-G	G-Y	G-Y	G
SiO_2	49.48	53.51	51.72	46.30
TiO_2	0.24	0.35	0.30	0.46
Al_2O_3	7.39	4.94	6.43	8.30
Cr_2O_3	0.01	0.03	0.00	0.04
FeO*	16.88	13.65	12.90	17.00
MnO	0.27	0.43	0.37	0.45
MgO	10.66	13.49	11.64	10.53
CaO	12.10	12.10	12.35	12.05
Na_2O	0.70	0.23	0.28	0.93
K_2O	0.09	0.16	0.33	0.46
Total	97.80	98.89	96.33	96.52
		O=23		
Si	7.280	7.621	7.556	6.987
Ti	0.026	0.038	0.033	0.052
Al^{IV}	0.720	0.379	0.444	1.013
Al^{VI}	0.562	0.451	0.664	0.464
Cr	0.001	0.003	0	0.005
Fe	2.077	1.626	1.576	2.146
Mn	0.034	0.052	0.046	0.058
Mg	2.338	2.862	2.535	2.368
Ca	1.907	1.847	1.933	1.948
Na	0.199	0.063	0.079	0.271
K	0.017	0.030	0.062	0.089

* Total iron as FeO

+ B:Brown, Bl:blue, G:green, Y:yellow

(Continued)

Sample no.	91100907	91100907	91100907	M720
Colour+	B	G	G	Bl-G
SiO_2	44.88	45.46	49.09	51.21
TiO_2	1.45	0.94	0.69	0.30
Al_2O_3	7.91	9.71	4.63	6.43
Cr_2O_3	0.00	0.01	0.00	0.03
FeO*	22.47	22.25	21.94	15.79
MnO	0.60	0.45	0.69	0.36
MgO	8.04	6.79	9.66	12.57
CaO	10.86	11.57	10.31	11.56
Na_2O	0.88	0.83	0.53	0.62
K_2O	0.66	0.84	0.25	0.11
Total	97.74	98.84	97.78	98.97
		O=23		
Si	6.876	6.836	7.407	7.381
Ti	0.167	0.106	0.078	0.032
Al^{IV}	1.126	1.137	0.593	0.619
Al^{VI}	0.303	0.590	0.230	0.474
Cr	0	0.001	0	0.003
Fe	2.879	2.809	2.768	1.904
Mn	0.077	0.057	0.089	0.043
Mg	1.836	1.528	2.171	2.700
Ca	1.784	1.872	1.666	1.785
Na	0.260	0.243	0.155	0.173
K	0.129	0.161	0.049	0.020

* Total iron as FeO

+ B:brown, Bl:blue, G:green, Y:yellow

(Continued)

Sample no.	M624	M624	M575	M681
Colour+	Bl-G	Bl-G	G	G
SiO_2	51.84	51.53	53.43	44.24
TiO_2	0.20	0.26	0.32	0.78
Al_2O_3	4.27	3.28	3.83	12.13
Cr_2O_3	0.26	0.18	0.00	0.00
FeO*	15.81	15.35	14.92	17.46
MnO	0.43	0.42	0.50	0.31
MgO	12.88	13.28	12.32	9.11
CaO	12.15	12.21	12.74	11.40
Na_2O	0.49	0.47	0.22	1.57
K_2O	0.14	0.10	0.08	0.46
Total	98.48	97.09	98.35	97.45
		O=23		
Si	7.563	7.594	7.715	6.626
Ti	0.022	0.029	0.035	0.087
Al^{IV}	0.464	0.406	0.285	1.374
Al^{VI}	0.268	0.164	0.366	0.768
Cr	0.030	0.021	0	0
Fe	1.922	1.893	1.802	2.188
Mn	0.053	0.052	0.061	0.039
Mg	2.791	2.918	2.561	2.033
Ca	1.893	1.928	1.971	1.830
Na	0.138	0.136	0.063	0.455
K	0.026	0.020	0.015	0.087

* Total iron as FeO

+ B:brown, Bl:blue, G:green, Y:yellow

(Continued)

Sample no.	M681	M681	M275	M275	M763
Colour+	G(Core)	G(Rim)	G-B	G-B	G-B
SiO_2	43.32	43.43	48.44	50.83	40.57
TiO_2	0.68	0.50	0.12	0.05	1.75
Al_2O_3	12.05	12.99	7.02	3.78	7.44
Cr_2O_3	0.00	0.01	0.16	0.00	0.06
FeO*	18.51	17.85	19.20	17.87	26.59
MnO	0.29	0.28	0.31	0.35	0.18
MgO	9.04	8.54	9.85	11.68	5.68
CaO	11.17	11.33	12.23	12.37	10.47
Na_2O	1.67	1.55	0.55	0.44	2.27
K_2O	0.42	0.41	0.24	0.10	1.07
Total	97.15	96.89	98.13	97.46	96.08
			O=23		
Si	6.554	6.555	7.213	7.552	6.573
Ti	0.077	0.057	0.014	0.006	0.214
Al^{IV}	1.446	1.445	0.787	0.448	1.421
Al^{VI}	0.704	0.867	0.445	0.214	
Cr	0	0.001	0.019	0	0.007
Fe	2.342	2.253	2.391	2.220	3.603
Mn	0.037	0.036	0.039	0.044	0.025
Mg	2.037	1.920	2.185	2.586	1.370
Ca	1.811	1.832	1.951	1.969	1.818
Na	0.491	0.453	0.160	0.128	0.714
K	0.080	0.079	0.046	0.018	0.221

* Total iron as FeO

+ B:brown, Bl:blue, G:green, Y:yellow

Table 3. Representative EPMA analyses of clinopyroxene.

Sample no.	91101506	91100902	M575	M575	M763
SiO_2	52.31	51.12	53.39	52.80	51.00
TiO_2	0	0.03	0.53	0.37	0.36
Al_2O_3	0.46	0.36	1.45	2.08	2.25
Cr_2O_3	0.02	0	0.01	0.13	0.00
FeO*	14.7	12.67	11.2	13.73	13.72
MnO	0.47	0.63	0.56	0.37	0.28
MgO	9.78	10.43	13.83	13.52	16.37
CaO	23.95	23.4	17.34	15.30	14.26
Na_2O	0.16	0.25	0.35	0.43	0.22
K_2O	0	0	0.09	0.56	0.02
Total	101.22	98.89	98.75	99.29	98.48
			O=6		
Si	1.986	1.98	2.007	1.991	1.935
Ti	0	0.001	0.015	0.010	0.010
Al^{IV}	0.014	0.016		0.009	0.065
Al^{VI}	0.007		0.064	0.083	0.036
Cr	0.001	0	0	0.004	0
Fe	0.447	0.411	0.352	0.433	0.435
Mn	0.015	0.021	0.018	0.012	0.009
Mg	0.554	0.602	0.775	0.760	0.926
Ca	0.974	0.971	0.699	0.618	0.580
Na	0.011	0.018	0.025	0.031	0.016
K	0	0	0.004	0.027	0.001

* Total iron as FeO

Table 4. Representative EPMA analyses of muscovite and biotite.

Sample no.	M103	M5(i)	M70	M799	M702
Minerals	Muscovite				Biotite
SiO_2	46.49	45.70	47.96	51.58	37.18
TiO_2	0.76	0.17	0.40	0.28	2.46
Al_2O_3	36.44	37.04	32.95	25.23	13.07
Cr_2O_3	0.07	0.00	0.07	0.00	0.18
FeO*	0.65	0.81	2.34	5.50	19.88
MnO	0.00	0.02	0.01	0.02	0.08
MgO	0.85	0.66	1.52	2.57	11.86
CaO	0.00	0.00	0.00	0.00	0.04
Na_2O	0.53	1.30	0.23	0.03	0.00
K_2O	10.18	8.99	10.12	9.75	9.88
Total	95.96	94.68	95.60	94.95	94.64
	O=22				O=22
Si	6.108	6.063	6.365	6.967	5.755
Ti	0.075	0.017	0.040	0.028	0.286
Al^{IV}	1.892	1.937	1.635	1.033	2.245
Al^{VI}	3.752	3.857	3.521	2.984	0.141
Cr	0.008	0	0.007	0	0.023
Fe	0.071	0.089	0.260	0.621	2.573
Mn	0	0.002	0.001	0.002	0.011
Mg	0.166	0.130	0.301	0.517	2.737
Ca	0	0	0	0	0.007
Na	0.135	0.334	0.058	0.009	0
K	1.705	1.523	1.714	1.679	1.951

* Total iron as FeO

Table 5. Representative EPMA analyses of epidote.

Sample no.	M711	M720	M666B
SiO_2	38.47	38.52	37.99
TiO_2	0.16	0.15	0.10
Al_2O_3	22.93	22.95	24.74
Cr_2O_3	0.00	0.00	0.00
Fe_2O_3*	12.67	12.80	11.75
MnO	0.20	0.05	0.12
MgO	0.10	0.00	0.06
CaO	22.70	22.65	23.35
Na_2O	0.02	0.00	0.01
K_2O	0.07	0.00	0.01
Total	97.32	97.13	98.13
	O=25		
Si	6.137	6.148	6.130
Ti	0.018	0.018	0.012
Al^{IV}			
Al^{VI}	4.313	4.319	4.706
Cr	0	0	0
Fe	1.520	1.538	1.586
Mn	0.027	0.007	0.016
Mg	0.024	0	0.014
Ca	3.879	3.874	4.038
Na	0.007	0	0.004
K	0.015	0	0.002

* Total iron as Fe_2O_3

Table 6. Representative EPMA analyses of chlorite.

Sample no.	M5(i)	M624	M575	M585	M666B
SiO_2	25.81	26.60	26.16	25.29	28.93
TiO_2	0.03	0.04	0.00	0.01	0.04
Al_2O_3	23.89	19.15	18.59	20.10	19.65
Cr_2O_3	0.02	0.00	0.04	0.10	0.00
FeO*	23.89	27.84	28.88	26.00	22.72
MnO	0.36	0.37	0.41	0.40	0.38
MgO	14.49	15.03	14.00	15.43	16.09
CaO	0.00	0.01	0.04	0.03	0.12
Na_2O	0.00	0.00	0.00	0.00	0.05
K_2O	0.03	0.00	0.00	0.00	0.33
Total	88.51	88.80	88.14	87.66	88.31
			O=28		
Si	5.320	5.607	5.606	5.429	5.940
Ti	0.004	0.006	0	0.001	0.006
Al^{IV}	2.680	2.393	2.394	2.571	2.060
Al^{VI}	3.126	2.365	2.303	2.457	2.697
Cr	0.003	0	0.010	0.016	0
Fe	4.119	4.845	5.175	4.613	3.901
Mn	0.063	0.066	0.075	0.072	0.067
Mg	4.453	4.722	4.472	4.880	4.923
Ca	0	0.003	0.009	0.007	0.026
Na	0	0	0	0	0.020
K	0.008	0	0	0	0.086

* Total iron as FeO

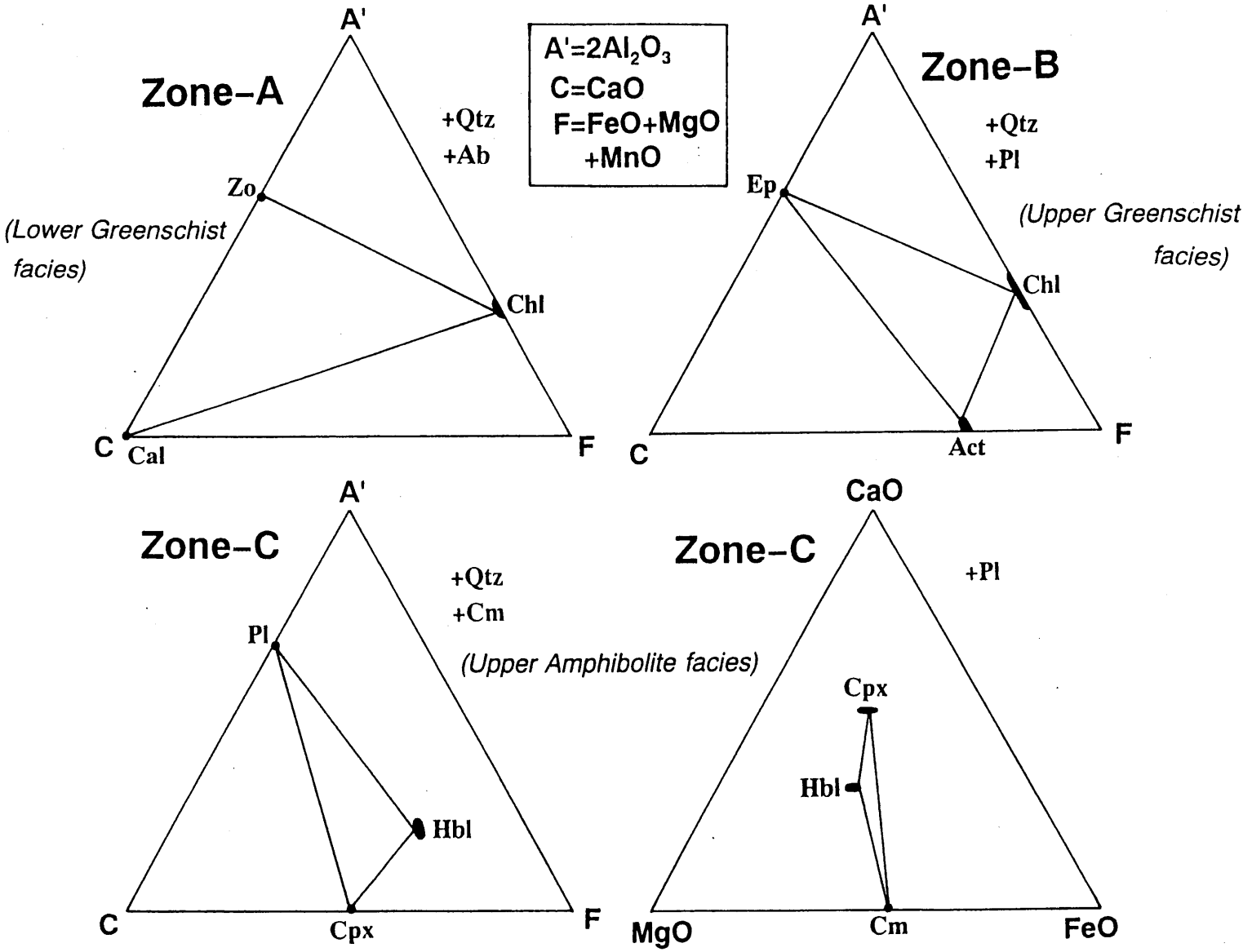

Fig. 4. A'-C-F and CaO-MgO-FeO diagrams of the contact-metamorphosed mafic rocks.

Table 7. Modal compositions and magnetic susceptibilities of the granitic rocks.

(3000 pts., vol. %)

	MH-91101101	MH-91101801	MH-91100509	MH-91101405	MH-91100901	MH-91100304	MH-91101402	MH-911012
Quartz	11.1	13.8	11.7	25.1	22.9	22.5	4.8	12.6
Alkali-feldspar	25.7	20.1	14.8	14.2	7.6	16.7	12.4	< 0.1
Plagioclase	31.7	43.7	44.6	55.6	57.9	50.6	63.3	57.5
Biotite	7.4	0.8	12.8	4.4	4.9	3.1	0.4	6.6
Hornblende	20.0	17.7	12.5	-	3.9	5.2	14.1	19.8
Clinopyroxene	0.6	-	2.4	-	-	-	0.2	-
Iron ores	2.2	1.9	0.3	0.3	1.4	0.2	1.9	1.6
Accessories*	1.3	2.0	0.8	0.5	1.4	1.6	2.8	1.9

*Apatite, allanite, sphene and zircon.

Magnetic susceptibilities of the granitic rock.

$\times 10^{-3}$SI	19.6	14.5	0.31	3.98	24.8	1.73	31.0	0.50

Table 8. Petrography of the granitic rocks.

(i)Maragoli (Kisian) granite

MH-91101101: Clinopyroxene bg. biotite-hornblende quartz-monzonite.
Texture: Coarse-grained & porphyritic (phenocrystic microcline & plagioclase) with basaltic enclaves.

Mineral	Morphology	Grain size (mm)	Microstructure & remarks
Quartz	Anhedral	<1.5	Mosaic
Alkali-feldspar	Subhedral - anhedral	10.0-0.2	Microcline perthite. Poikilitically contains biotite & quartz blobs.
Plagioclase	Euhedral - subhedral	8.0-0.3	Zoned & polysynthetically twinned. Sericitized in core parts.
Hornblende	Euhedral - subhedral	<3.0	Z=olive green. Some include Cpx in core part. Twinned.
Biotite	Subhedral	<2.0	Chloritized

MH-91101801: Biotite bg. hornblende quartz-monzodiorite.
Texture: Coarse-grained & porphyritic (phenocrystic microcline & plagioclase).

Mineral	Morphology	Grain size (mm)	Microstructure & remarks
Quartz	Anhedral	<2.0	Mosaic
Alkali-feldspar	Euhedral - anhedral	13.0-0.2	Microcline perthite. Poikilitically contains plagioclase & quartz blobs.
Plagioclase	Euhedral - subhedral	7.0-1.0	Strongly zoned & polysynthetically twinned. Sericitized & saussuritized in core parts.
Hornblende	Euhedral - anhedral	3.5-0.5	Z=olive green.
Biotite	Subhedral	<1.0	Chloritized

(Continued)

MH-91100509: Clinopyroxene-hornblende-biotite quartz-monzodiorite.
Texture: Medium-grained & massive.

Mineral	Morphology	Grain size (mm)	Microstructure & remarks
Quartz	Anhedral	<1.5	Mosaic
Alkali-feldspar	Subhedral - anhedral	2.5-0.2	Microcline perthite
Plagioclase	Euhedral - subhedral	3.0-0.4	Zoned & polysynthetically twinned. Sericitized in core parts.
Hornblende	Mantling & replacing Cpx		Z=olive green (Actinolite?). Z=very pale green (Cummingtonite?). Later stage than Cpx.
Clinopyroxene	Subhedral	5.0-0.3	Augite
Biotite	Anhedral	<1.0	Intergrown with Cpx and Amphi. Partly chloritized.

(ii)Asembo (Bondo) granite

MH-91101405: Biotite granodiorite.
Texture: Medium-grained & massive.

Mineral	Morphology	Grain size (mm)	Microstructure & remarks
Quartz	Anhedral	3.0-0.2	Mosaic
Alkali-feldspar	Subhedral - anhedral	1.8-0.2	Orthoclase perthite
Plagioclase	Euhedral - subhedral	3.0-0.2	Strongly zoned & polysynthetically twinned. Sericitized in core parts.
Biotite	Subhedral - anhedral	1.2-0.2	Partly chloritized.

(Continued)

MH-91100901: Hornblende-biotite granodiorite.
Texture: Medium-grained & massive with small basaltic enclaves.

Mineral	Morphology	Grain size (mm)	Microstructure & remarks
Quartz	Anhedral	<1.8	
Alkali-feldspar	Anhedral	<0.8	Microcline perthite
Plagioclase	Euhedral - subhedral	3.0-0.3	Strongly zoned & polysynthetically twinned. Sericitized in core parts.
Hornblende	Euhedral - subhedral	<2.5	Z=olive green. Intergrown with biotite.
Biotite	Subhedral	1.5-0.2	

(iii)Mumias (Kitoshi, Kakamega) granite

MH-91100304: Biotite-hornblende granodiorite.
Texture: Coarse-grained & porphyritic (phenocrystic microcline & plagioclase).

Mineral	Morphology	Grain size (mm)	Microstructure & remarks
Quartz	Anhedral	2.0-0.2	Mosaic
Alkali-feldspar	Subhedral - anhedral	5.0-0.5	Microcline
Plagioclase	Euhedral	7.0-2.0	Strongly zoned & polysynthetically twinned. Sericitized in core parts.
Hornblende	Euhedral - subhedral	2.0-0.2	Z=olive green.
Biotite	Anhedral	1.0-0.2	Chloritized

(Continued)

(iv)Microgranite

MH-91101402: Clinopyroxene-biotite bg. hornblende quartz-monzodiorite.
Texture: Fine-grained & faintly gneissose.

Mineral	Morphology	Grain size (mm)	Microstructure & remarks
Quartz	Anhedral	<0.5	Interstitial
Alkali-feldspar	Anhedral	1.0-0.3	Orthoclase perthite
Plagioclase	Euhedral - subhedral	2.5-0.5	Strongly zoned & polysynthetically twinned. Saussuritized in core parts.
Hornblende	Subhedral	2.2-0.2	Z=olive green. Poikilitically includes Cpx & biotite blobs.

MH-91101205: Biotite-hornblende quartzdiorite.
Texture: Fine-grained.

Mineral	Morphology	Grain size (mm)	Microstructure & remarks
Quartz	Anhedral	1.0-0.2	
Plagioclase	Euhedral - subhedral	5.0-0.5	Completely sericitized.
Hornblende	Subhedral	1.5-0.1	Z=brownish green.
Biotite	Subhedral	1.5-0.1	Completely chloritized.

Table 9. Bulk chemical compositions of the granitic rocks.

	Maragoli Gr.						Asembo Gr.			
Sample no.	1101209	9101801	9100506	91101101	91100509	94080408	91100901	91101405	91101802	91101204
SiO_2	64.71	63.01	66.02	62.79	60.75	67.11	66.16	71.28	69.38	65.12
TiO_2	0.32	0.43	0.30	0.38	0.60	0.34	0.41	0.16	0.17	0.38
Al_2O_3	15.78	15.09	16.32	15.80	15.26	15.27	15.90	14.99	15.99	14.43
Fe_2O_3	3.69	4.30	2.97	4.21	5.70	2.82	3.17	1.51	1.82	3.21
MnO	0.06	0.07	0.06	0.07	0.10	0.05	0.04	0.03	0.04	0.05
MgO	2.03	2.65	0.93	2.40	3.49	1.80	1.53	0.34	0.41	1.06
CaO	3.59	4.05	2.27	3.90	5.11	2.60	4.05	1.76	2.10	2.52
Na_2O	4.73	4.72	5.27	5.50	3.59	4.89	4.70	4.69	4.82	7.03
K_2O	3.33	3.70	4.42	3.68	3.28	3.29	1.98	3.32	3.29	2.02
P_2O_5	0.21	0.31	0.12	0.31	0.25	0.16	0.12	0.04	0.06	0.14
Total	98.45	98.33	98.68	99.04	98.13	98.33	98.06	98.12	98.08	95.96

(Continued)

	Asembo Gr.		Mumias Gr.		Micro Gr.					Diorite	
Sample no.	94080306	94080406	91100301	91100304	91100801	91101402	91101501	94080205	91101205	91101201	94080206
SiO_2	64.89	63.12	57.59	64.39	65.95	59.33	69.31	66.17	55.75	68.87	52.57
TiO_2	0.38	0.41	0.74	0.26	0.37	0.51	0.24	0.34	1.05	0.31	0.43
Al_2O_3	16.19	16.08	16.22	17.54	16.54	16.28	15.43	16.00	18.07	15.52	15.54
Fe_2O_3	3.78	3.94	7.30	2.77	3.23	5.50	2.17	3.16	7.86	2.70	7.82
MnO	0.05	0.09	0.12	0.05	0.05	0.09	0.03	0.05	0.12	0.05	0.13
MgO	1.58	2.32	3.77	1.48	1.08	2.73	1.09	0.67	2.61	0.76	7.85
CaO	3.96	2.73	5.38	3.26	3.35	4.85	2.72	3.47	6.70	2.82	9.95
Na_2O	2.30	4.52	3.63	5.26	5.03	5.66	4.80	4.99	3.87	4.71	3.96
K_2O	2.10	4.70	3.38	3.34	2.08	2.51	2.26	2.38	1.36	2.20	1.05
P_2O_5	0.13	0.21	0.30	0.14	0.12	0.39	0.06	0.13	0.25	0.09	0.06
Total	95.36	98.12	98.43	98.49	97.80	97.85	98.11	97.36	97.64	98.03	99.36

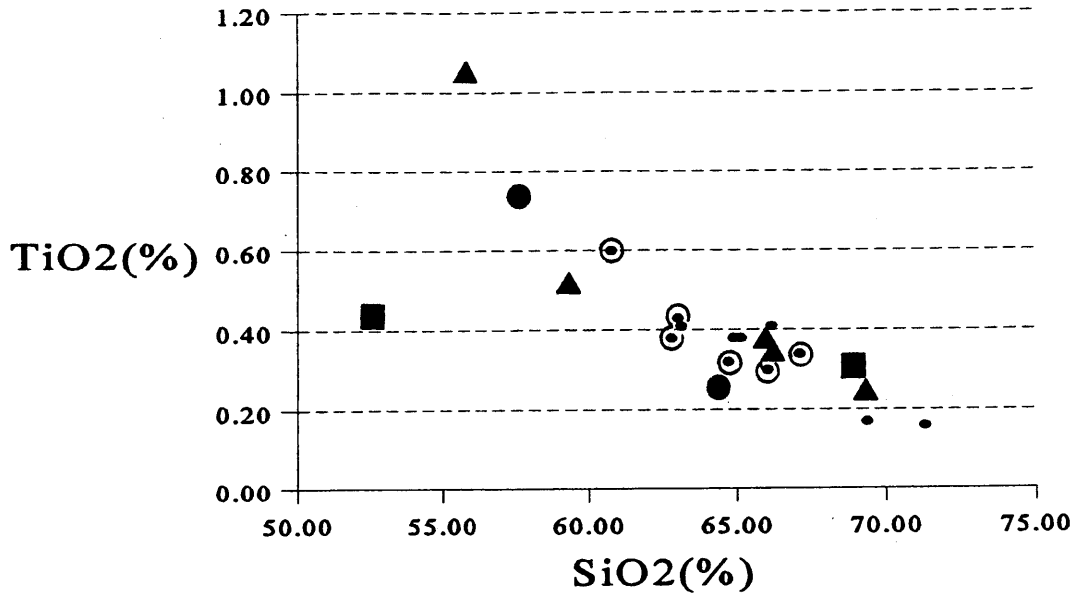

⊙ Maragoli Gr.
• Asembo Gr.
● Mumias Gr.
▲ Micro Gr.
■ Diorite

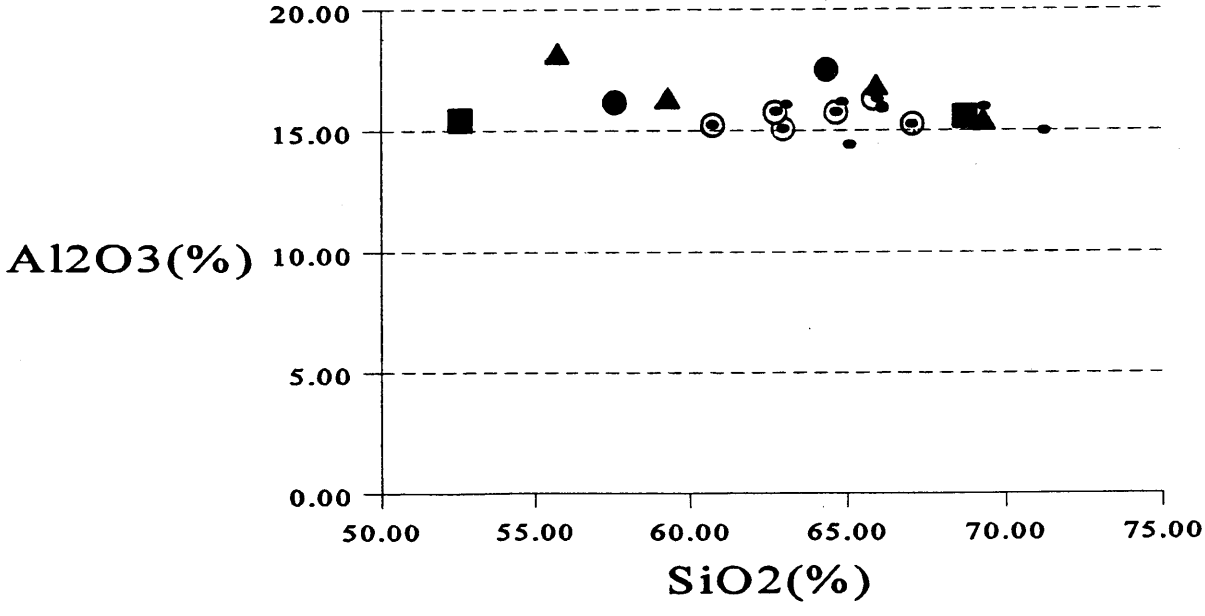

Fig. 5. TiO_2 -SiO_2 and Al_2O_3-SiO_2 diagrams.

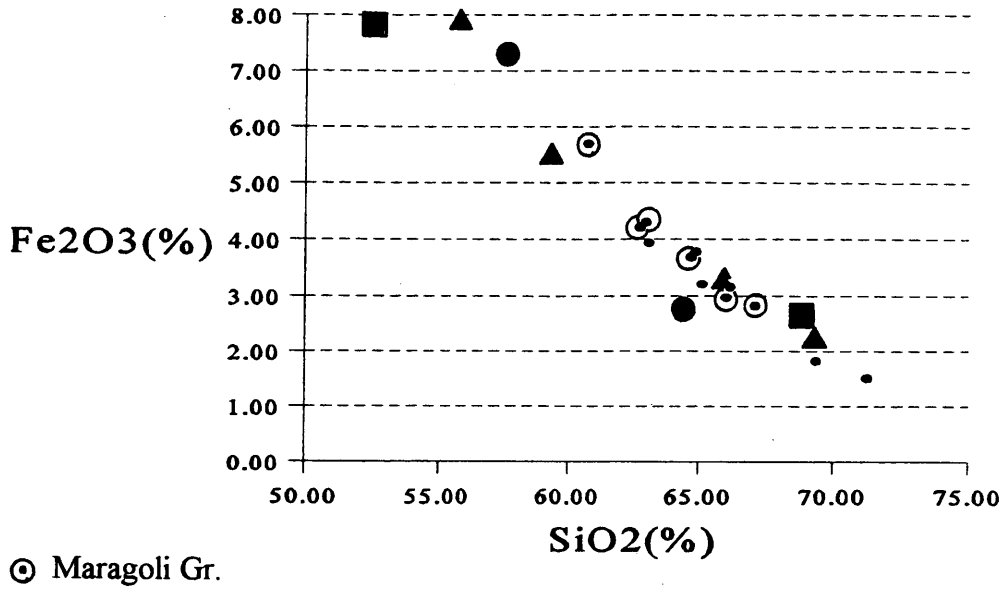

⊙ Maragoli Gr.

• Asembo Gr.

● Mumias Gr.

▲ Micro Gr.

■ Diorite

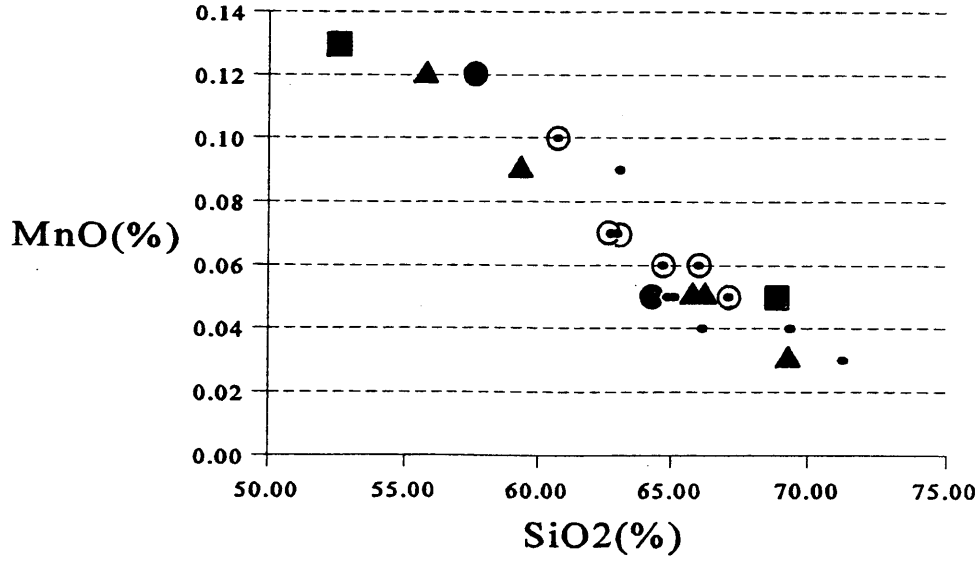

Fig. 6. Fe_2O_3-SiO_2 and MnO-SiO_2 diagrams.

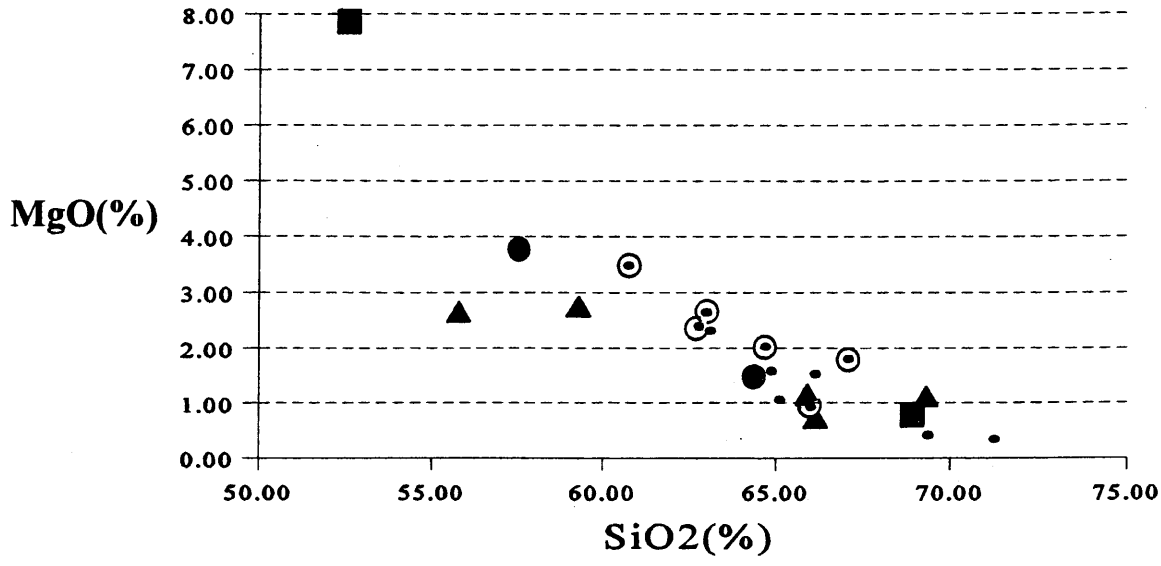

⊙ Maragoli Gr.

• Asembo Gr.

● Mumias Gr.

▲ Micro Gr.

■ Diorite

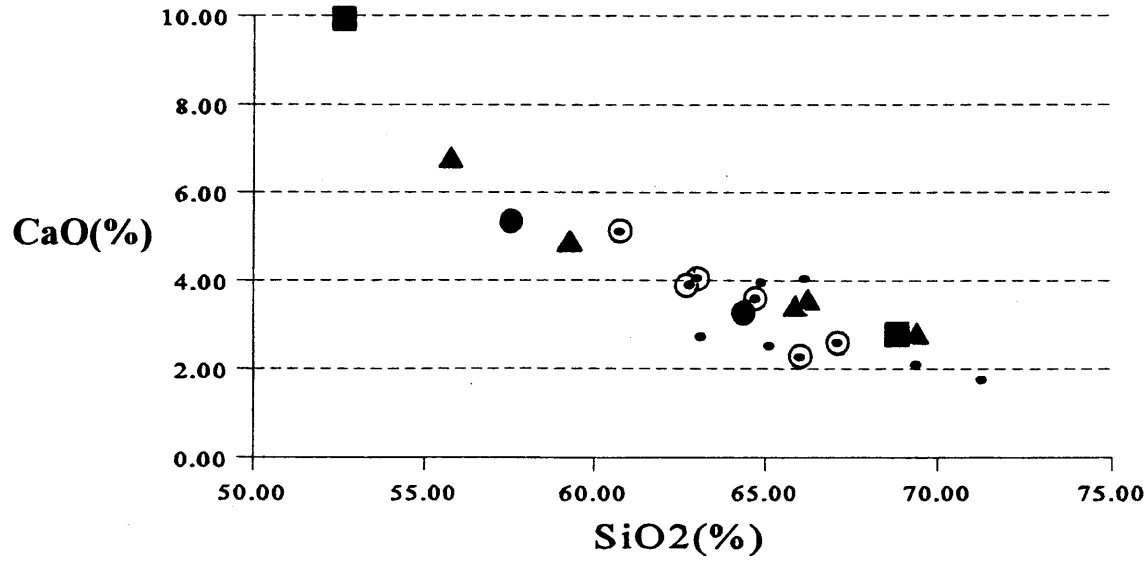

Fig. 7. $MgO\text{-}SiO_2$ and $CaO\text{-}SiO_2$ diagrams

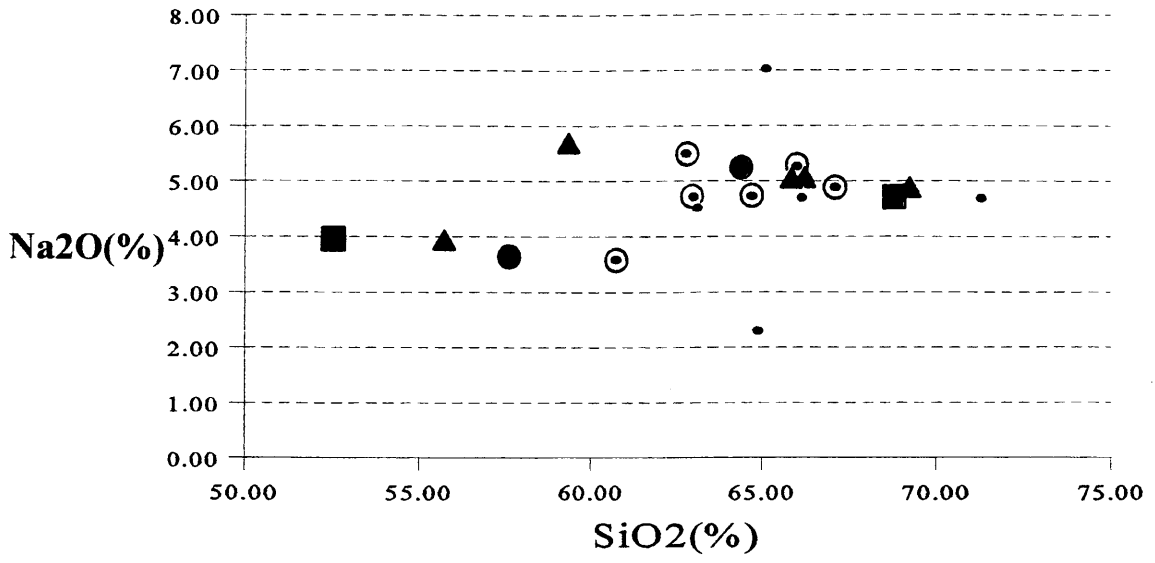

⊙ Maragoli Gr.
• Asembo Gr.
● Mumias Gr.
▲ Micro Gr.
■ Diorite

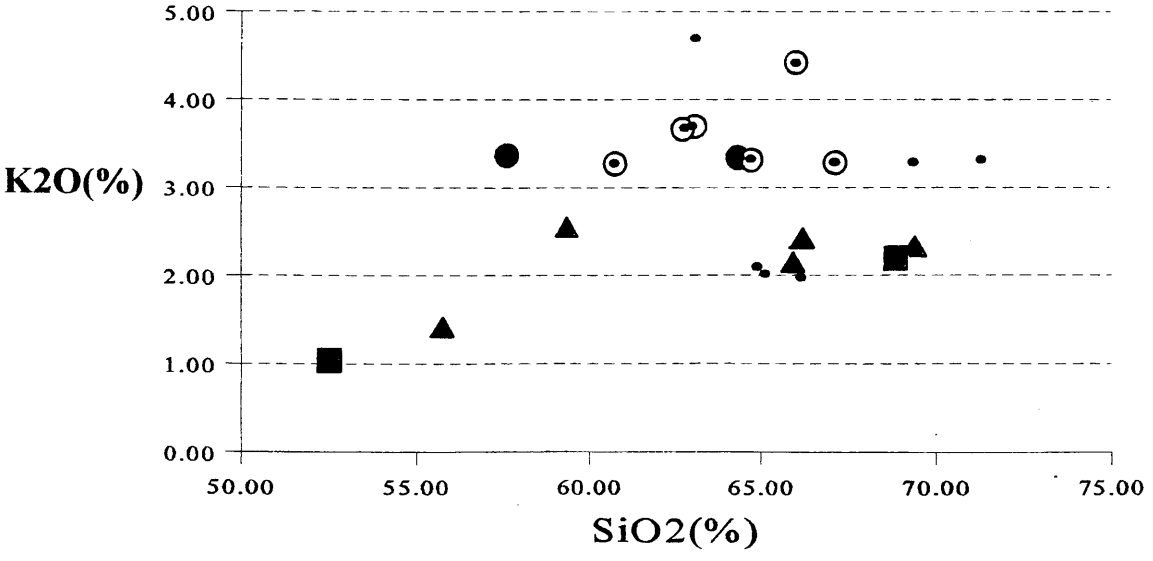

Fig. 8. Na_2O-SiO_2 and K_2O-SiO_2 diagrams.

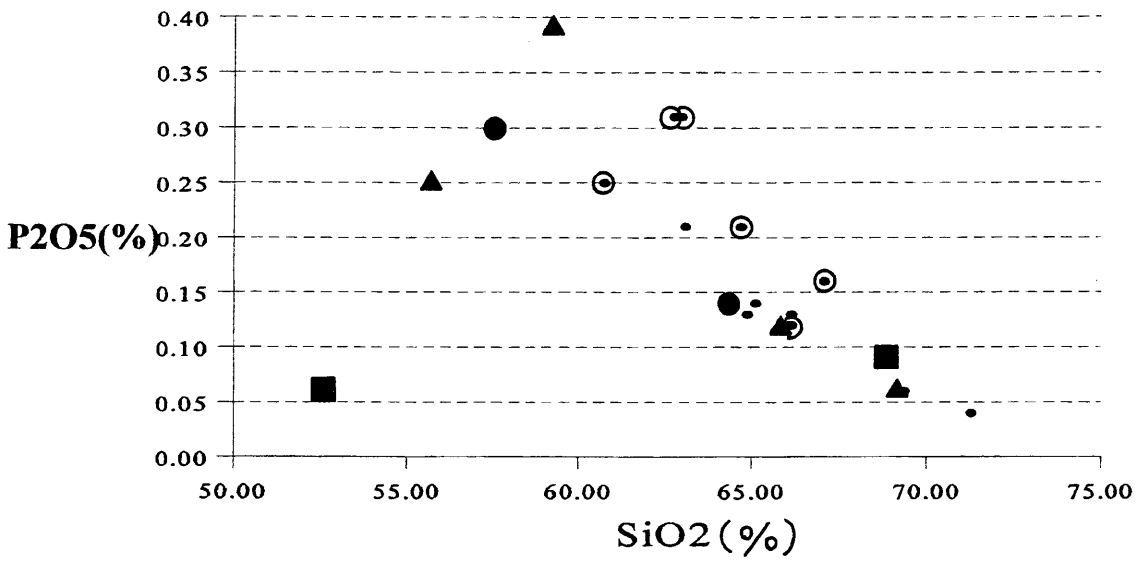

Fig. 9. P_2O_5-SiO_2 diagram.

- ⊙ Maragoli Gr.
- • Asembo. Gr.
- ● Mumias Gr.
- ▲ Micro Gr.
- ■ Diorite

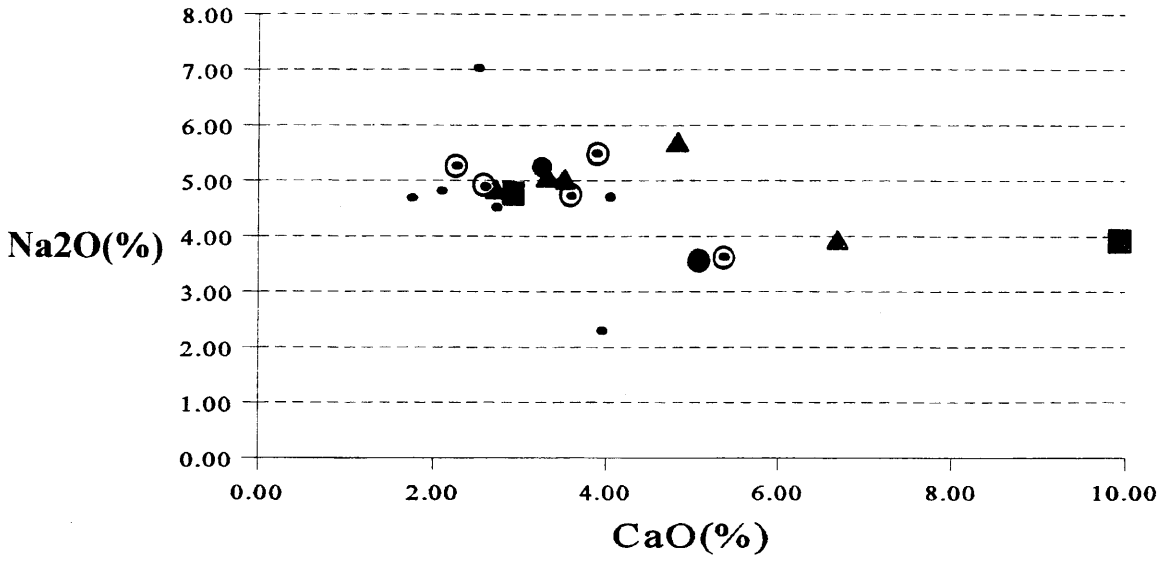

⊙ Maragoli Gr.
• Asembo Gr.
● Mumias Gr.
▲ Micro Gr.
■ Diorite

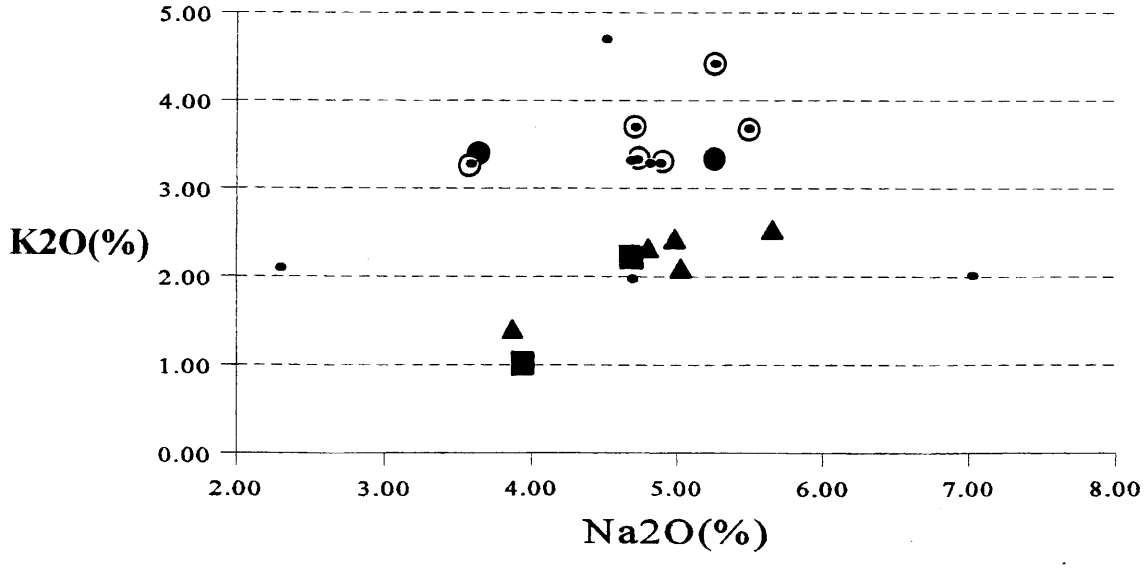

Fig. 10. Na_2O-CaO and K_2O-Na_2O diagrams.

The paper submitted to the Journal of African Earth Sciences

PETROLOGY, GEOCHEMISTRY AND PETROGENESIS OF SOME ARCHAEAN GRANITES FROM THE ARCHAEAN GREENSTONE BELT TO THE NORTH OF LAKE VICTORIA, WESTERN KENYA

Norbert Opiyo-Akech*[1] and Mitsuo Hoshino*[2]

*[1] Department of Geology, University of Nairobi, P.O.Box 30197, Nairobi, Kenya
*[2] School of Informatics and Sciences, Nagoya University, Nagoya 464-01, Japan

Abstract

The greenstone belt of western Kenya is part of what is commonly referred to as the Tanganyika Shield. The two groups of rock sequences recognized in this sequence are the Nyanzian and the Kavirondian groups. The rocks found in these groups are diverse, with dominant volcanics in the Nyanzian and dominant sedimentary rocks in the Kavirondian group. Geochemical studies on these granites comparable to those of granites found in present day continental arc environments. In this study the petrology, geochemistry and some petrogenetic models are presented. The study shows that these rocks are related in their petrogenesis. It shows that it is possible to model the petrogenesis of these granites by crystal fractionation from a source similar to the Nyanzian calc-alkaline volcanics found in close proximity to these rocks.

Introduction

The granites found in this area are typical of the TTG sequences found in most granite greenstone sequences of the world. They are intruded into both the Nyanzian group of metavolcanics and the Kavirondian group of metasediments. They range in age from the micro-granites that are assumed to be pre-Nyanzian (>2.8Ga) to some post-Kavirondian (<2.4Ga) granites (Opiyo-Akech, 1991).

Sampling on these granites was done to include all representative sample s (Fig. 1) from the pre-Nyanzian microgranites to the three plutons (1)Kisian, Maragoli or Maseno granites, (2)Mumias, Kitoshi or Kakamega granites, (3)Asembo or Bondo granites as earlier described by Opiyo-Akech (1992). Based on regional mapping and outcrop patterns, these granitic rocks are grouped into three main subdivisions, namely;

1) Mumias (Kitoshi, Kakamega) granites
2) Kisian (Maragoli, Maseno) granites
3) Asembo (Bondo) granites

The Mumias granites covers the northern section of the area and is the most extensive granite body in this part of the belt. It extends from around Mumias town and extends westwards into Uganda. To the east from Mumias it extend to beyond Kakamega town. The Kisian

granite extends from Maragoli in Vihiga district southwestwards to Kamuga bay. The Asembo granite lies to the west of Kisian granite and extends from west of Kombewa, westwards into Asembo and Uyoma.

Sample analysis

The Modal composition was determined by means of the Swift automatic point counter, Model E at Nagoya University. Initial major and trace elements analyses were carried out at the University of Leicester, England, with further analyses being carried out at the Geological Survey of South Africa using X-ray fluorescence (XRF) techniques. Mineral chemistry analysis were carried out at the Geological Survey of South Africa using an electron microprobe.

Petrology and petrochemistry

The Mumias and the Kisina granites, in the field are characterized by large tors that dominate the landscape. It is noted that there are considerable chemical and petrological variations ranging from granodiorites, through tonalites, adamellites, to coarse and medium grained granites to microgranites, all within close proximity and grading into one another. These granitic intrusions in this belt are of the TTG sequence with typical representative mineralogical compositions and magnetic susceptibilities as listed on Table 1.

On the basis of the three major subdivisions into the Mumias granites, Kisian granites and the Asembo granites, brief petrographic descriptions of representative rock samples from each of the major plutons are tabulated below.

Geochemistry

Geochemistry indicates that these granites are of igneous origin and any sedimentary fingerprints are probably caused by contamination (Opiyo-Akech, 1988). The initial $^{87}Sr/^{86}Sr$ ratios of 0.7012 to 0.7007 for the Mumias granites (Dodson et al., 1975) and 0.7015 for the Kisian granites (Bell and Dodson, 1981) are indicative of these rocks being mantle derived.

Comparative studies of these granites reveal a concurrence with the expected trends of rocks from the same source or sources with similar composition (Opiyo-Akech, 1988). The Harker variation diagrams show normal trends expected from involvement of fractional crystallization. Apart from the wide scatter of points for Na_2O and K_2O which are probably due to the mobility of these elements during low grade metamorphism and weathering. All the other major elements show the expected fractionation downward trend with increase in silica, apart from Al2O3 which shows a varying trend by first increasing and then decreasing rapidly in the more acid varieties, Listed on Tables 5 and 6 are representative samples from

the Mumias and Kishian granites.

In the Kisian granites, tonalites and adamellites are the dominant rock types, while the Mumias granites are dominated by massive porphyritic granites ranging in composition from granodiorites to true granites.

Petrographic, chemical and field observations of the variations within the three main granite bodies indicate that the Asembo graintes (Table 7) exhibits the most restricted compositional range, with most of the samples analysed falling within the tonalite field. The Kisian granites show the widest spread with the sequences being represented.

Classification of these rocks (Fig.2) was carried out using the R1-R2 classification method of Debon and Le Fort (1982). On this diagram and similar discriminant diagrams these rocks range in composition from granodiorites, through monzodiorites, tonalites, quartz monzonites, monzonites to true granites.

The major elements apparent differentiation trends are also indicated in the trace elements and rare earth elements (REEs) trends. Plots of various selected trace elements against SiO_2, show the behaviour of these elements in respect to the incompatibility in these systems (Opiyo-Akech, 1992a). Assuming that SiO_2 increases with differentiation, then Ba, Sr and Y are strongly compatible whereas Rb and Nb are incompatible. The elements like Ba and Sr that enter the K sites early in the fractionation of feldspars are noted to decrease rapidly with an increase in silica concentration. This behaviour probably reflects the influence of accessory minerals such as zircon and apatite.

On the chondrite normalised plots of the REEs (Fig. 3), the Mumias and Kisian granites are observed to have higher REE contents than the Asembo granites. But the overall patterns are similar with enrichment of LREEs and a negative Eu anomaly. In this respect Eu exhibits a similar behaviour to Sr in keeping with the fact that plagioclase affects both elements in a similar manner during differentiation.

Magmatism and tectonic setting

Of importance on this study is the determination of magma type and the possible evolutionary trends taken by the evolving magma. The studies indicate that these are calc-alkaline rocks. The AFM diagram (Fig. 4). shows a clear calc-alkaline trend for the rocks from the different areas.

The cation plots as used by Batchelor and Bowden (1985), from Debon and Le Fort (1982) and Debon et al. (1987) and La Roche (1984, Fig. 5) also display a metaluminous calc-alkaline trend that is in general agreement with the AFM diagram.

On the tectono-magmatic association diagram of Batchelor and Bowden (1985), the majority of these rocks plot on the post-collision trend, with a few samples particularly those from the Mumias granites plotting on the pre-collision intrusions may illustrate different time episodes of magmatism. This is also indicated on the field relationships with the presence of granitic boulders within the Kavirondian conglomerates.

On trace elements discriminant diagrams, the patterns observed are those typical of (VAG) calc-alkaline granites, and are similar to those observed elsewhere in the belt (Davis and Condie, 1977). Plots of Rb versus Y+Nb and Nb versus Y of Pierce et al. (1984) place these rocks in the field of volcanic arc granites (VAG) (Fig. 6a,b).

From the chemical analyses it is possible to model the variations from the least evolved to the most evolved granites. The models invoked (Table 8) involve crystal fractionation of rocks from a similar source, in which the crystal fractionation is assumed to be the major influencing determinant in differentiation. When modelling, the choice of samples to be modelled are restricted to rocks within the groupings of the Mumias, Kisian and Asembo granites. In each case, the most primitive member of each group is assumed to representative of the parental magma from which all the differentiates are derived.

The model employed for the major elements uses the least squares method. The model gives an indication of the possibility of deriving a particular rock from a more primitive one by assessing the residues (squared residuals R^2). This is done by fractionating the possible crystal phases from the system. This works out the percentages of the various mineral phases fractionated and gives the squares of the residuals. Low R^2 indicates a good fit and indications of the possibility of obtaining the more evolved rocks from the more primitive source rocks.

In modelling, a stepwise approach on samples from the same sequence is taken. The modelling starts from with the least evolved samples and a progressive stepwise analysis is followed until the compositions of the most fractionated member is obtained. The phases fractionating are also changed to reflect the important fractionating phases in the assemblages. The R^2 values obtained for these rocks within the various groups are consistent and reasonable (Opiyo-Akech, 1992b), but are higher than the values obtained for volcanic in this locality, a factor which could be attributed to the mobility of the alkalies.

The rare earth elements (REEs) are also used in modelling fractionation trends in these rocks. The models employ the distribution coefficient (D_{values}) obtained from Henderson (1984). From this fractionation model it has been possible to model the generation of the more evolved rocks within the various groups by crystallizing to varying proportions, different mineral phases. For comparison purposes the percentages of mineral assemblages used are those of values calculated from the major element models. The patterns produced from these models indicate that it is possible to derive the more fractionated varieties of these rocks from

the more primitive assemblages within the same units by fractionation. Fairly good fits are generated using mineral proportions taken from the least squares modelling for the major elements.

Summary and conclusions

In classifying these rocks it is noted that there is a wide compositional range from monzodiorites, tonalites, granodiorites to granites. This variation is clearly observed in the petrography and the chemical analyses. On discriminant plots (Fig. 6), they are noted to be calc-alkaline, and further discrimination places them on the volcanic arc granites (VAG). On the multi-element plots, they have a high LILE/HFSE ratios and a negative Nb anomaly indicative of subduction zone granites.

From these geochemical evidence, it is concluded that the granites are mantle derivatives, with their chemistry being altered by crustal contaminants. The initial $^{87}Sr/^{86}Sr$ ratios (Bell and Dodson, 1981) is close to that of modern day mantle. The scatter of plots on the Harker diagrams (Opiyo-Akech, 1992a), probably reflect mixing between mantle derived material and crustal contaminants, with a possible contribution from low grade metamorphism and weathering.

In conclusion, it is noted that these rocks are derived from the mantle and are closely related in their geochemistry and petrogenesis. The models show that it is possible to generate rocks of more evolved composition from the least evolved varieties by fractionation.

Acknowledgements

This study is supported partly by the Grant-in-Aid from JSPS and Monbusho (no. 07640638).

REFERENCES

Batchelor, R.A. and Bowden, P., 1985. Petrogenetic interpretation of granitoid rock series using multicationic parameters. Chemical Geology, **48**, 43-55.

Bell, K. and Dodson, M.H., 1981. Geochronology of the Tanzanian Shield. Journal of Geology, **89**, 109-128.

Davis. Jr., P.A. and Condie, K.C., 1977. Trace elements studies of Nyanzian greenstone belt, western Kenya. Geochim. Cosmochim. Acta, **40**, 553-556.

Debon, F. and Le Fort, P., 1982. A chemical-mineralogical classification of common plutonic rocks and associations. Trans. R. Soc. Edinburgh. Earth Sci., **73**, 135-149.

Debon, F. and Le Fort, P., Dautel, D., Sonet, J. and Zimmerman, J.L., 1987. Granites of

western Karakorum and northern Kohistan (Pakistan). A composite mid-Cretaceous to upper-Cenozoic magmatism. Lithos, **20**, 19-40.

Dodson, M.H., Gledhill, A.R., Shackleton, R.M. and Bell, K., 1975. Age differences between Archaean cratons of eastern and souther Africa. Nature, **154**, 315-318.

Harris, C., 1983. The petrology of lavas and associated plutonic inclusions of Ascensions island. Journal of Petrology, **24**, 424-470.

Henderson, P., 1982. Inorganic geochemistry. Pergamon Press.

Opiyo-Akech, N., 1988. Geology and geochemistry of the late Archaean greenstone associations, Maseno area, Kenya. Unpublished Ph. D. thesis, 149pp.

Opiyo-Akech, N., 1992a. Tectono-magmatic emplacement of the Kenyan granite-greenstones: Geochemical evidences from the Maseno area, western Kenya. Afr. Jour. Sci. Tech., Series B, **6**, 51-57.

Opiyo-Akech, N., 1992b. Geochemical evidence for the emplacement of the Archaean greenstones volcanics from the Maseno area, western Kenya. Afr. Jour. Sci. Tech., Series B, **6**, 51-57.

Pearce, J.A., Lippard, S.J. and Roberts, S., 1984. Characteristics and tectonic significance of supracrustal zone ophiolites. In: Marginal Basin Geology (Special publication of the Geological Society, London), Edited by Kokelaar, B.P. and Howells, M.F.), pp. 77-94.

Figure captions

Figure 1: Map showing the locations of the three major granite bodies to the north of L. Victoria.

Figure 2: Classification of the granites on the R1-R2 diagram of Debon and Le Fort (1982).

Figure 3: Average chondrite normalized REE plots for the granites from the three bodies.

Figute 4: The AFM diagram showing the trend of the granites.

Figure 5: Distribution of the Maseno granites as displayed on the Aluminous index versus the dark minerals in the rocks.

Figure 6: Y+Nb versus Rb and Y versus Nb diagrams showing the tectonic setting. (after Pearce et al., 1984-a and Harris 1983-b)

Figure 7: Example of a REE fractionation model for the granites.

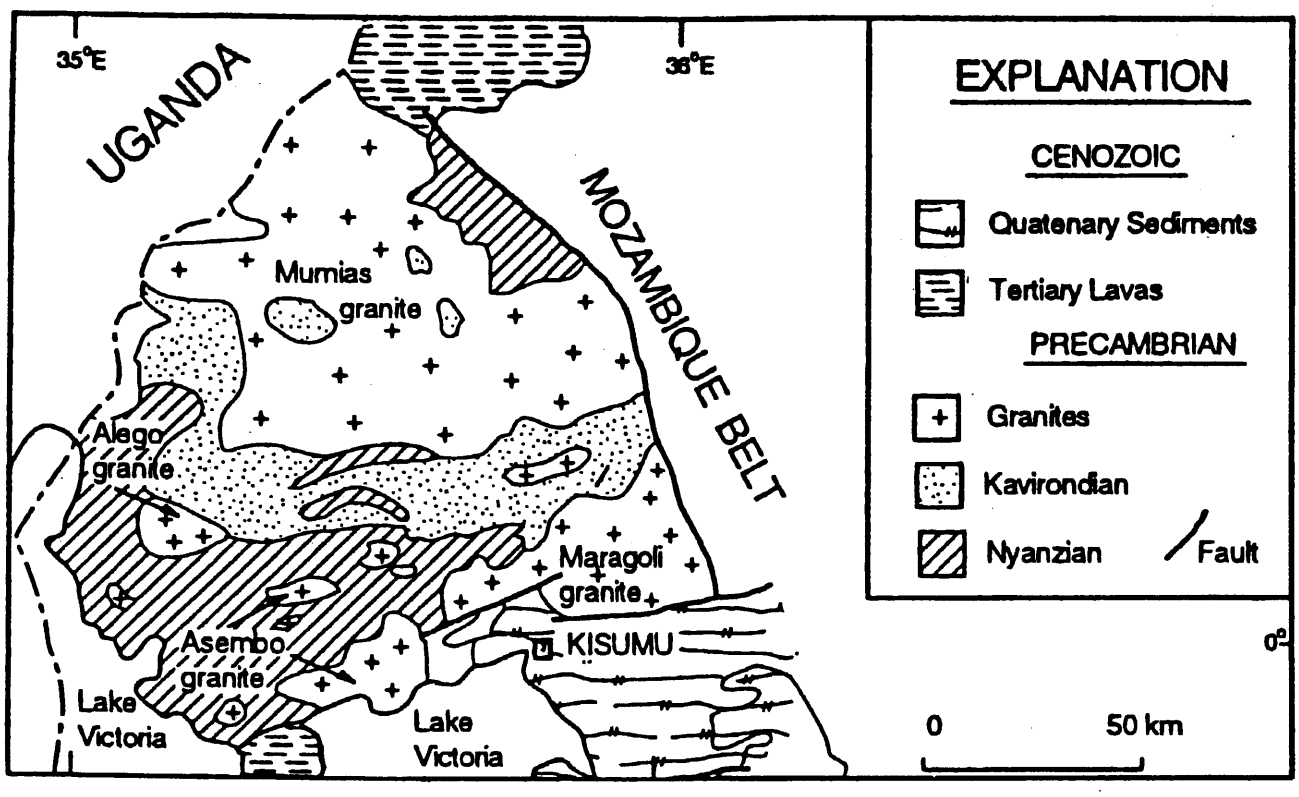
35°E
36°E
UGANDA
MOZAMBIQUE BELT
Mumias granite
Alego granite
Maragoli granite
Asembo granite
KISUMU
Lake Victoria
Lake Victoria
0°
0
50 km
EXPLANATION
CENOZOIC
Quatenary Sediments
Tertiary Lavas
PRECAMBRIAN
Granites
Kavirondian
Nyanzian
Fault

Fig. 1

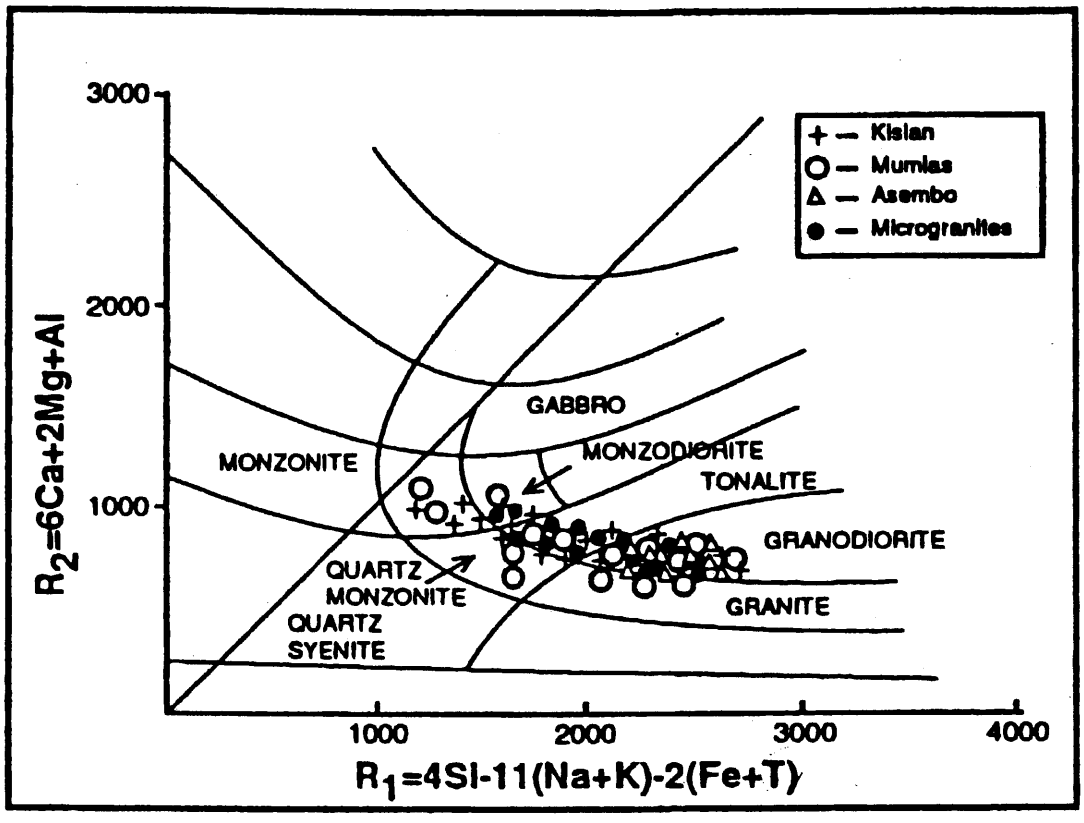
3000
2000
1000
R_2=6Ca+2Mg+Al
+ — Kisian
O — Mumias
△ — Asembo
● — Microgranites
GABBRO
MONZODIORITE
MONZONITE
TONALITE
GRANODIORITE
QUARTZ
MONZONITE
QUARTZ
SYENITE
GRANITE
1000
2000
3000
4000
R_1=4Si-11(Na+K)-2(Fe+T)

Fig. 2

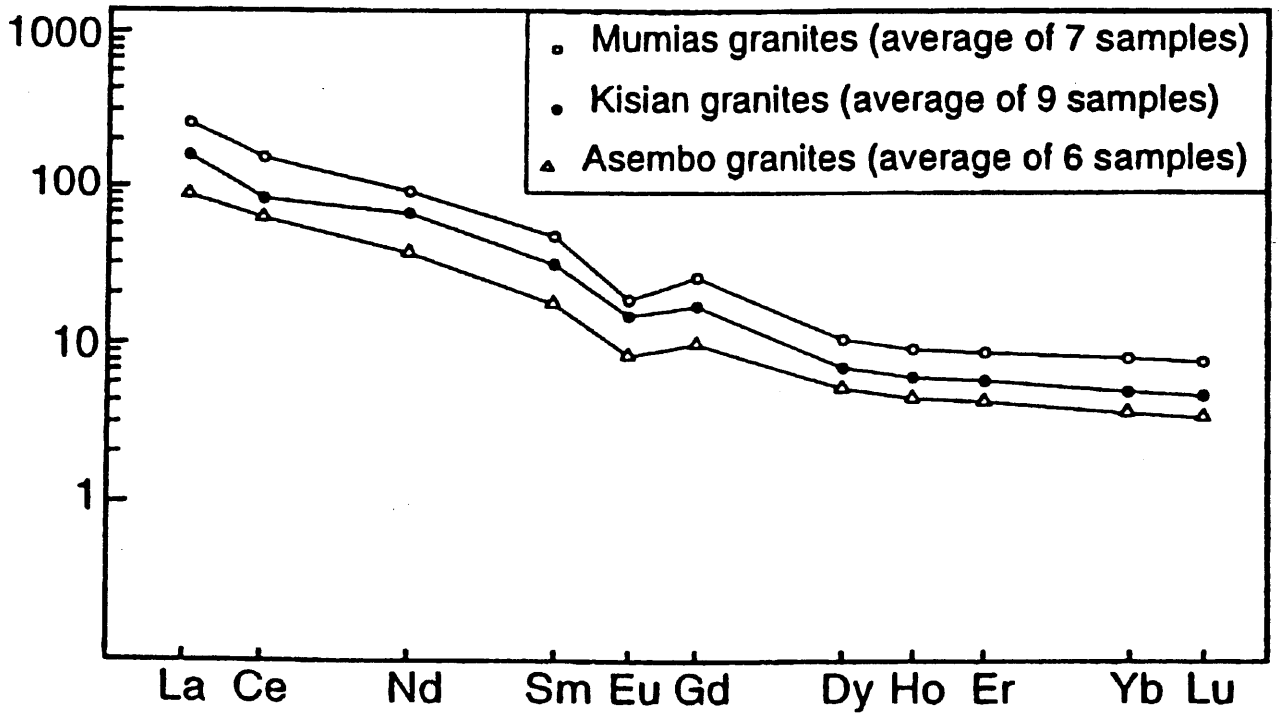
1000
100
10
1
Mumias granites (average of 7 samples)
Kisian granites (average of 9 samples)
Asembo granites (average of 6 samples)
La Ce Nd Sm Eu Gd Dy Ho Er Yb Lu

Fig. 3

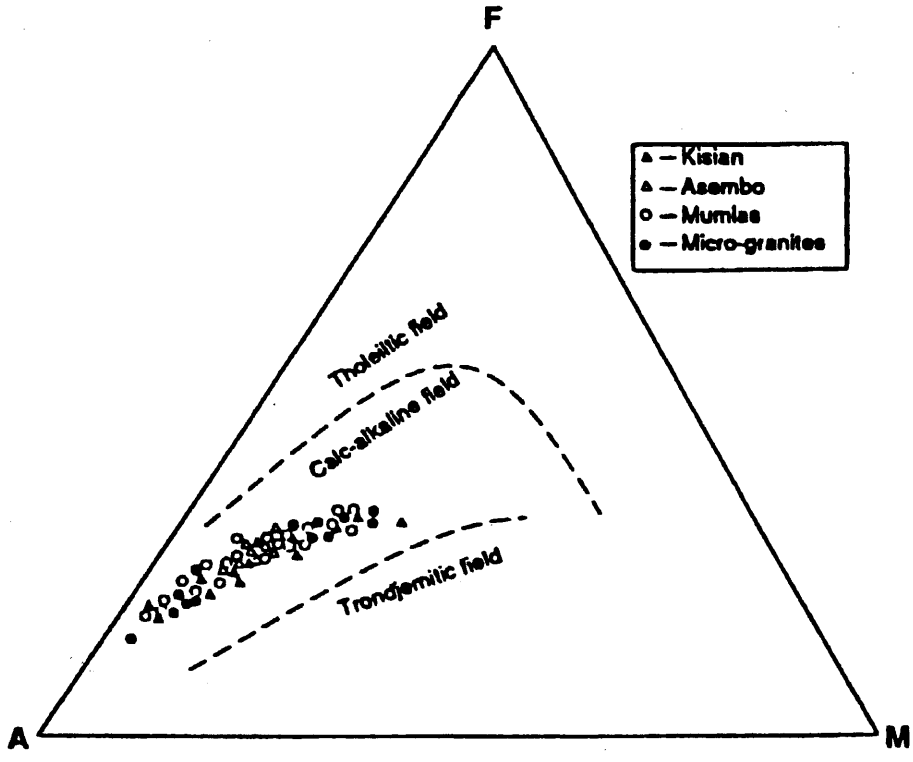
F
A
M
▲ — Kisian
▲ — Asembo
○ — Mumias
● — Micro-granites
Tholeiitic field
Calc-alkaline field
Trondjemitic field

Fig. 4

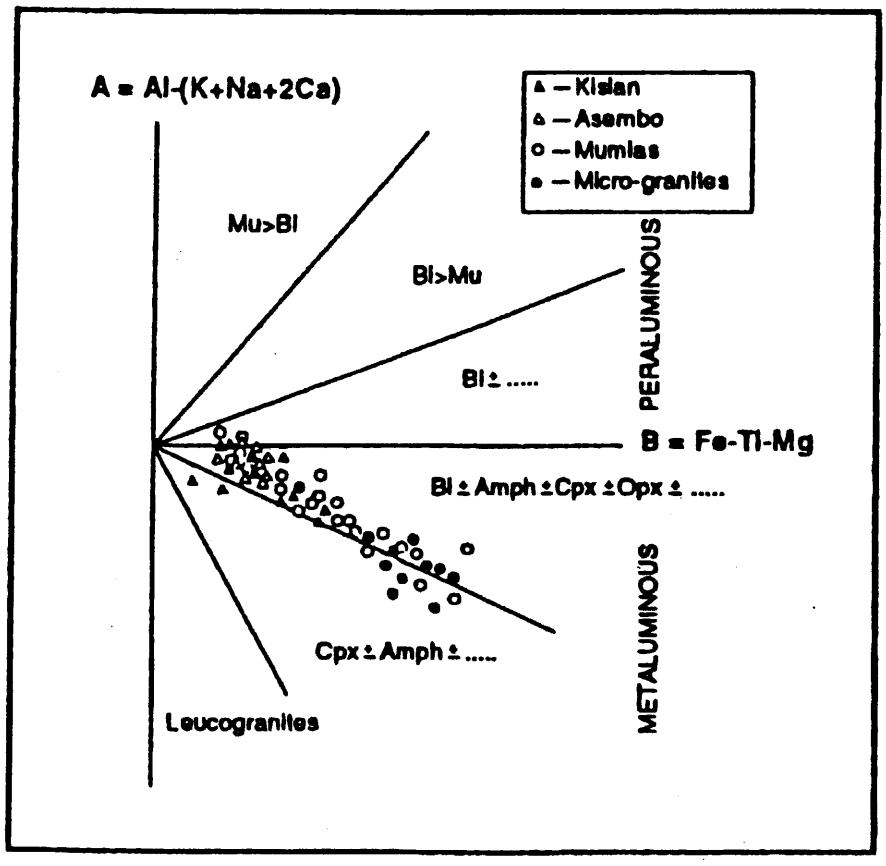
A = Al-(K+Na+2Ca)
▲ — Kisian
△ — Asembo
○ — Mumias
● — Micro-granites
Mu>Bl
Bl>Mu
Bl ± .....
PERALUMINOUS
B = Fe-Ti-Mg
Bl ± Amph ± Cpx ± Opx ± .....
Cpx ± Amph ± .....
Leucogranites
METALUMINOUS

Fig. 5

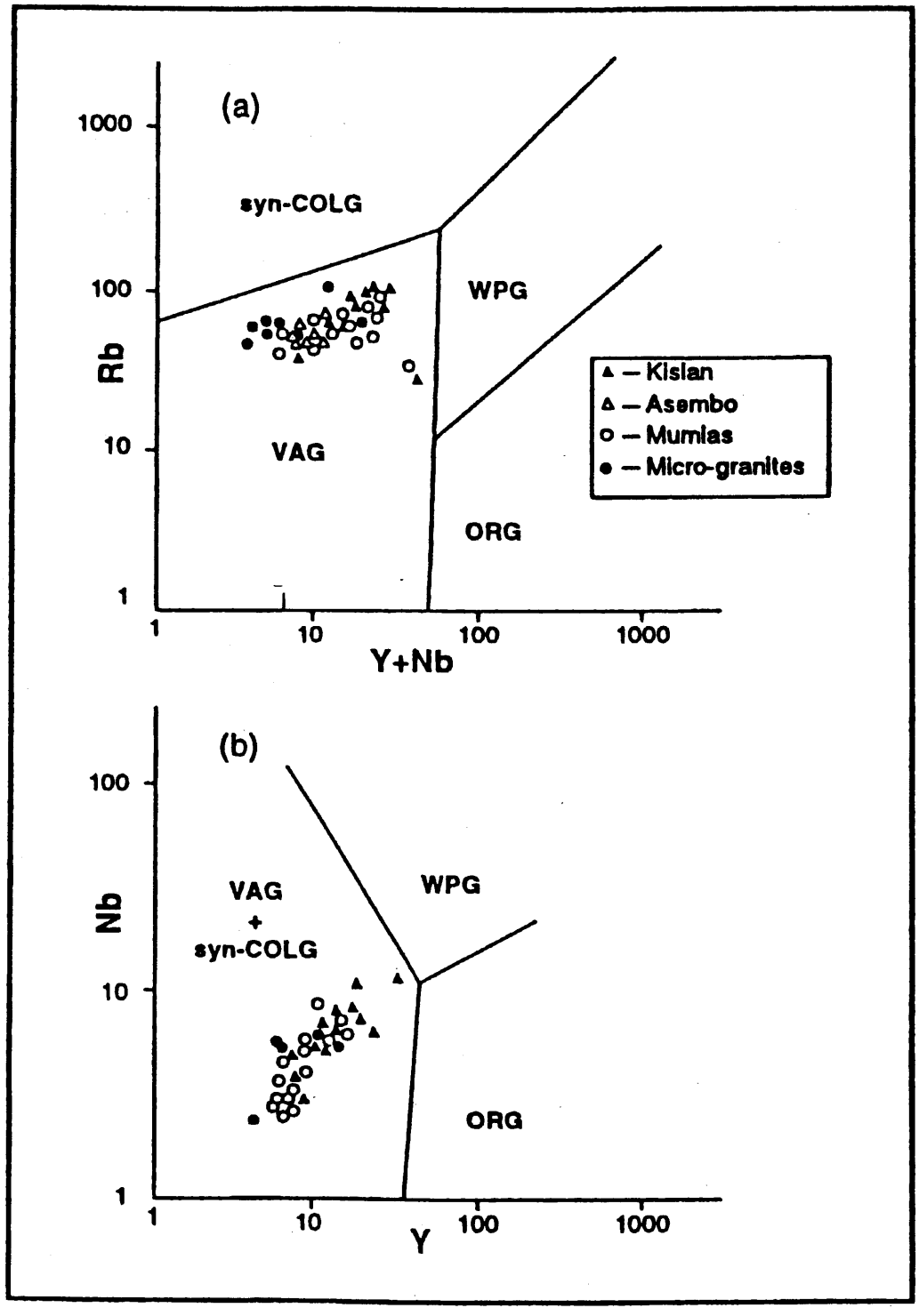
(a)
1000
100
10
1
Rb
syn-COLG
WPG
VAG
ORG
▲ — Kisian
△ — Asembo
○ — Mumias
● — Micro-granites
1
10
100
1000
Y+Nb
(b)
100
10
1
Nb
VAG
+
syn-COLG
WPG
ORG
1
10
100
1000
Y

Fig. 6

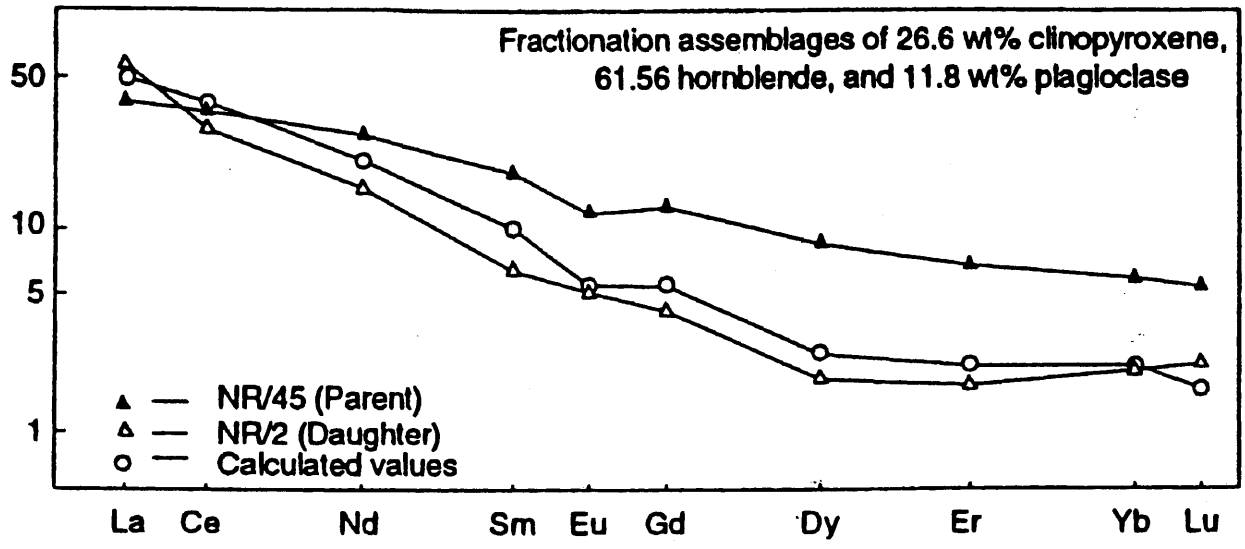
Fractionation assemblages of 26.6 wt% clinopyroxene,
61.56 hornblende, and 11.8 wt% plagioclase
50
10
5
1
▲ — NR/45 (Parent)
△ — NR/2 (Daughter)
○ — Calculated values
La
Ce
Nd
Sm
Eu
Gd
Dy
Er
Yb
Lu

Fig. 7

Table 1. Modal composition of some granitic rocks in the western Kenya greenstone belt.
(3000 pts., vol. %)

Sample No.	91101101	91101801	91100509	91101405	91100901	91100304	91101403	91101205
Quartz	11.1	13.8	11.7	25.1	22.9	22.5	4.8	12.6
Alkali feldspar	25.7	20.1	14.8	14.2	7.6	16.7	12.4	<0.1
Plagioclase	31.7	43.7	44.6	55.6	57.9	50.6	63.3	57.5
Biotite	7.4	0.8	12.8	4.4	4.9	3.1	0.4	6.6
Hornblende	20.0	17.7	12.5	-	3.9	5.2	14.1	19.8
Clinopyroxene	0.6	-	2.4	-	-	-	0.2	-
Iron ores	2.2	1.9	0.3	0.3	1.4	0.2	1.9	1.6
Accessories*	1.3	2.0	0.8	0.5	1.4	1.6	2.8	1.9

*Apatite, allanite, sphene and zircon

Magnetic susceptibilities of these granitic rocks

$\times 10^{-3}$ SI	19.6	14.5	0.31	3.98	14.8	1.73	31.0	0.50

Table 2(a). Kisian (Maragoli) granite. Location/Sample No. MH-91101101
Petrographical rock type: Quartz-monzonite

Mineral	Morphology	Grain size (mm)	Microstructure and remarks
Quartz	Anhedral	<1.5	Mosaic
Alkali feldspar	Subhedral-Anhedral	10.0-0.2	Microcline perthite. Poikilitically contains biotite and quartz blobs
Plagioclase	Euhedral-Subhedra	8.0-0.3	Zoned, polysynthetically twinned. Sericitized cores
Hornblende	Euhedral-Subhedral	<3.0	Z=olive green. Some include Cpx in core. Twinned
Biotite	Subhedral	<2.0	Chloritized

Texture: Coarse grained & porphyritic (phenocrystic microcline and plagioclase) with basaltic enclaves.

Table 2(b). Kisian (Maragoli) granite. Location/Sample No. MH-91101801
Petrographical rock type: Quartz-monzodiorite

Mineral	Morphology	Grain size (mm)	Microstructure and remarks
Quartz	Anhedral	<2.0	Mosaic
Alkali feldspar	Euhedral-Anhedral	13.0-0.2	Microcline perthite. Poikilitically contains plagioclase and quartz blobs
Plagioclase	Euhedral-Subhedral	7.0-1.0	Strongly zoned, polysynthetically twinned. Sericitized and saussuritized cores
Hornblende	Euhedral-Anhedral	3.5-0.5	Z=olive green.
Biotite	Subhedral	<1.0	Chloritized

Texture: Coarse grained & porphyritic (phenocrystic microcline and plagioclase)

Table 2(c). Kisian (Maragoli) granite. Location/Sample No. MH-91100509
Petrographical rock type: Quartz-monzodiorite

Mineral	Morphology	Grain size (mm)	Microstructure and remarks
Quartz	Anhedral	<1.5	Mosaic
Alkali feldspar	Subhedral-Anhedral	2.5-0.2	Microcline perthite.
Plagioclase	Euhedral-Subhedra	3.0-4.0	Zoned, polysynthetically twinned. Sericitized cores
Hornblende	Mantling & replacing Cpx		Z=olive green(Act.?) Z=pale green(Cumm.?) Later stage than Cpx
Clinopyroxene	Subhedral	5.0-0.3	Augite
Biotite	Anhedral	<1.0	Intergrown with Cpx & Amphi. Partly chloritized

Texture: Medium grained and massive

Table 3. Mumias (Kitoshi, Kakamega) granite. Location/Sample No. MH-91100304
Petrographical rock type: Granodiorite

Mineral	Morphology	Grain size (mm)	Microstructure and remarks
Quartz	Anhedral	2.0-0.2	Mosaic
Alkali feldspar	Subhedral-Anhedral	5.0-0.5	Microcline
Plagioclase	Euhedral	7.0-2.0	Strongly zoned, polysynthetically twinned. Sericitized cores
Hornblende	Euhedral-Subhedral	2.0-0.2	Z=olive green.
Biotite	Anhedral	1.0-0.2	Chloritized

Texture: Coarse grained & porphyritic (phenocrystic microcline and plagioclase)

Table 4(a). Asembo (Bondo) granite. Location/Sample No. MH-91101405
Petrographical rock type: Granodiorite

Mineral	Morphology	Grain size (mm)	Microstructure and remarks
Quartz	Anhedral	3.0-2.0	Mosaic
Alkali feldspar	Subhedral-Anhedral	1.8-0.2	Orthoclase perthite.
Plagioclase	Euhedral-Subhedra	3.0-0.2	Strongly zoned, polysynthetically twinned.
Biotite	Subhedral-Anhedral	1.2-0.2	Partly chloritized

Texture: Medium grained and massive

Table 4(b). Asembo (Bondo) granite. Location/Sample No. MH-91100901
Petrographical rock type: Granodiorite

Mineral	Morphology	Grain size (mm)	Microstructure and remarks
Quartz	Anhedral	<0.8	
Alkali feldspar	Anhedral	<0.8	Microcline perthite.
Plagioclase	Euhedral-Subhedral	3.0-0.3	Strongly zoned, polysynthetically twinned. Sericitized cores
Hornblende	Euhedral-Subhedral	<2.5	Z=olive green. Intergrown with biotite
Biotite	Subhedral	1.5-0.2	

Texture: Medium grained & massive with small basaltic enclaves

Table 5. Chemical analysis of representative samples from the Kisian pluton.

Sample Number	103	107	108	104	45	105	106
SiO2	64.87	73.66	71.15	67.69	64.37	64.45	72.23
TiO2	0.50	0.23	0.32	0.36	0.46	0.43	0.43
Al2O3	15.53	14.58	15.31	15.17	15.75	15.43	15.32
Fe2O3	4.76	1.52	2.76	3.23	4.30	4.31	1.84
MnO	0.08	0.02	0.03	0.05	0.07	0.07	0.04
MgO	2.73	0.42	0.64	1.61	2.39	2.49	0.57
CaO	4.40	2.32	2.83	2.91	3.82	4.13	2.46
Na2O	4.22	4.92	5.53	4.57	5.10	5.52	5.50
K2O	3.23	2.66	1.74	0.22	3.95	3.45	2.68
P2O5	0.22	0.07	0.11	2.64	0.31	0.31	0.07
LOI	1.28	1.00	1.17	2.64	0.87	1.86	1.74
Total	100.54	100.40	100.42	100.38	100.52	100.59	101.14
V	82.0	19.9	27.0	47.0	63.0	60.0	60.0
Cr	71.0	29.0	11.6	30.0	55.0	50.0	52.0
Ni	25.0	3.1	16.4	15.9	25.0	26.0	26.0
Zn	64.0	24.0	39.0	49.0	63.0	61.0	61.0
Ga	19.4	17.8	22.0	19.5	19.5	21.0	20.0
Rb	105.0	73.0	63.0	131.0	122.0	88.0	89.0
Sr	637.0	436.0	407.0	719.0	825.0	779.0	776.0
Y	14.3	3.0	3.3	12.5	15.3	17.9	17.7
Zr	123.0	81.0	104.0	122.0	134.0	148.0	155.0
Nb	6.3	1.1	2.2	7.5	8.6	8.7	7.8
Ba	846.0	880.0	201.0	1277.0	961.0	697.0	693.0
La	39.0	14.8	19.9	40.0	51.0	52.0	50.0
Ce	73.0	16.3	22.0	74.0	104.0	91.0	90.0
Nd	33.0	4.5	7.4	33.0	48.0	42.0	43.0
Th	15.6	4.8	8.9	12.7	13.3	17.3	13.9

Table 6. Chemical analysis of representative samples from the Mumias pluton.

Sample Number	172	179	180	181	182	183	184
SiO2	68.83	72.72	68.05	66.50	68.69	69.43	66.68
TiO2	0.41	0.30	0.41	0.45	0.40	0.37	0.45
Al2O3	15.90	14.39	15.51	15.89	15.31	15.25	15.77
Fe2O3	2.83	1.96	3.23	3.66	3.13	2.75	3.72
MnO	0.05	0.03	0.06	0.06	0.05	0.04	0.07
MgO	1.07	0.49	1.45	1.77	1.36	1.11	1.79
CaO	2.81	1.45	2.98	3.49	2.80	2.48	3.48
Na2O	5.23	4.35	4.94	5.14	4.84	4.80	5.08
K2O	2.84	4.28	3.33	3.01	3.52	3.51	3.14
P2O5	0.17	0.14	0.21	0.23	0.22	0.16	0.25
H2O+	0.81	0.90	2.19	0.71	1.49	1.66	0.97
Total	99.72	100.11	100.17	100.20	100.32	99.84	100.43
V	42.0	21.0	46.0	55.0	43.0	38.0	54.0
Cr	18.1	7.5	29.0	36.0	24.0	25.0	33.0
Ni	7.5	3.9	14.0	17.4	11.6	12.6	15.0
Zn	61.0	47.0	60.0	64.0	59.0	55.0	65.0
Ga	22.0	20.0	20.0	20.0	20.0	20.0	20.0
Rb	85.0	213.0	122.0	92.0	134.0	151.0	94.0
Sr	875.0	344.0	687.0	801.0	677.0	531.0	843.0
Y	7.7	11.0	11.5	11.6	11.6	11.1	11.9
Zr	126.0	166.0	136.0	126.0	149.0	131.0	141.0
Nb	3.4	9.5	6.5	5.5	6.8	7.6	5.5
Ba	990.0	678.0	847.0	903.0	839.0	774.0	920.0
La	35.0	61.0	44.0	39.0	50.0	45.0	44.0
Ce	47.0	77.0	70.0	67.0	73.0	68.0	72.0
Nd	23.0	37.0	33.0	1.0	35.0	31.0	34.0
Th	2.0	25.0	11.2	6.6	10.6	19.1	3.3

Table 7. Chemical analysis of representative samples from the Asembo pluton.

Sample Number	12	118	119	120	115	116	117
SiO2	70.85	72.21	72.18	70.90	72.50	71.76	72.10
TiO2	0.23	0.32	0.27	0.39	0.29	0.33	0.32
Al2O3	14.19	14.99	15.39	15.57	15.02	15.32	15.16
Fe2O3	1.69	2.56	2.39	3.14	2.23	2.70	2.46
MnO	0.03	0.04	0.05	0.05	0.04	0.05	0.04
MgO	0.35	0.60	0.47	0.77	0.48	0.61	0.55
CaO	2.06	2.85	2.40	3.25	2.46	2.83	2.66
Na2O	4.85	4.81	5.25	4.87	5.04	4.98	5.00
K2O	5.55	2.04	2.23	1.80	2.27	2.02	2.17
P2O5	0.06	0.07	0.07	0.08	0.07	0.07	0.07
LOI	1.39	2.11	4.14	2.46	2.14	0.91	1.37
Total	99.86	100.49	100.70	99.92	100.40	100.67	100.53
V	16.1	28.0	21.0	37.0	23.0	28.0	27.0
Cr	6.5	5.2	4.0	6.4	5.0	5.2	5.3
Ni	4.3	4.8	2.9	4.2	4.2	4.0	4.2
Zn	38.0	42.0	49.0	48.0	45.0	46.0	46.0
Ga	21.0	19.4	20.0	20.0	20.0	20.0	20.0
Rb	77.0	60.0	81.0	46.0	72.0	62.0	65.0
Sr	236.0	268.0	283.0	300.0	248.0	284.0	259.0
Y	6.6	5.9	6.7	7.3	7.7	6.6	7.6
Zr	98.0	102.0	102.0	102.0	112.0	102.0	110.0
Nb	4.2	2.9	3.3	3.6	4.0	3.3	3.9
Ba	519.0	476.0	473.0	507.0	416.0	485.0	439.0
La	13.6	17.6	18.4	10.4	16.7	15.5	15.1
Ce	21.0	30.0	32.0	16.0	29.0	26.0	25.0
Nd	10.5	12.3	13.3	7.5	12.4	11.0	11.2
Th	1.6	1.4	8.7	7.6	4.3	5.9	5.1

Table 8: An example of a least squares model of fractionation as applied to the granites.

Model	Daughter NR/1	horn	bio	plag	Kspar	Calc-Parent	Parent NR/105	Residue
SiO_2	64.87	45.15	34.33	59.13	64.28	64.68	64.71	-0.03
TiO_2	0.50	1.25	3.63	0.03	0.00	0.34	0.45	-0.11
Al_2O_3	15.53	8.10	14.80	25.06	19.40	15.73	15.59	0.14
Fe_2O_3	4.76	2.10	2.48	0.05	0.34	4.43	4.18	0.25
MnO	0.08	0.45	0.35	0.00	0.00	0.06	0.07	-0.01
MgO	2.73	13.30	11.62	0.05	0.00	1.99	2.10	-0.11
CaO	4.40	12.84	1.56	7.44	0.48	4.00	3.88	0.12
Na_2O	4.22	0.66	0.65	6.89	2.74	4.24	4.61	-0.37
K_2O	3.23	0.32	8.16	0.32	11.80	3.61	3.59	0.02

Squared residual (R^2) = 0.2612